


Fall 2017

Surface Offset and Slip Rates for the Winter Rim Fault System in the Summer Lake Basin, Oregon

Jennifer Hall
jenniferhallcwu@gmail.com

Follow this and additional works at: <https://digitalcommons.cwu.edu/etd>

 Part of the [Geology Commons](#), [Geomorphology Commons](#), and the [Tectonics and Structure Commons](#)

Recommended Citation

Hall, Jennifer, "Surface Offset and Slip Rates for the Winter Rim Fault System in the Summer Lake Basin, Oregon" (2017). *All Master's Theses*. 900.
<https://digitalcommons.cwu.edu/etd/900>

This Thesis is brought to you for free and open access by the Master's Theses at ScholarWorks@CWU. It has been accepted for inclusion in All Master's Theses by an authorized administrator of ScholarWorks@CWU. For more information, please contact pingfu@cwu.edu.

SURFACE OFFSET AND SLIP RATES FOR THE WINTER RIM FAULT SYSTEM
IN THE SUMMER LAKE BASIN, OREGON

A Thesis

Presented to

The Graduate Faculty

Central Washington University

In Partial Fulfillment

of the Requirements of the Degree

Master of Science

Geological Sciences

by

Jennifer Michelle Hall

November 2017

CENTRAL WASHINGTON UNIVERSITY
Graduate Studies

We hereby approve the thesis of

Jennifer Michelle Hall

Candidate for the degree of Master of Science

APPROVED FOR THE GRADUATE FACULTY

Dr. Anne Egger, Committee Chair

Dr. Walter Szeliga

Dr. Lisa Ely

Dean of Graduate Studies

ABSTRACT

SURFACE OFFSET AND SLIP RATES FOR THE WINTER RIM FAULT SYSTEM IN THE SUMMER LAKE BASIN, OREGON

by

Jennifer Michelle Hall

November 2017

The 66-km-long Winter Rim Fault (WRF) system, located in the northwestern Basin and Range Province, encompasses several Holocene fault scarps within the Summer Lake basin that include the WRF system, a normal fault divided into three segments: Slide Mountain (SMF), Winter Ridge, and Ana River (ARF), and the newly-mapped Thousand Springs fault (TSF). The current least-compressive stress field is oriented $\sim 264^\circ$ (Crider, 2001). The USGS estimates a slip rate of 0.43 mm/yr, earthquake magnitudes of 6.5-7.19, and recurrence interval of 3.1 ka (Crone et al., 2009). However, these estimates are only based upon ARF and the unfavorably slip-oriented SMF. With high-resolution LiDAR, means to calculate a more inclusive slip rate estimate is possible, with fault scarps that cut radiocarbon-dateable tufa-coated paleoshorelines from Pleistocene Pluvial Lake Chewaucan. The faults have been active since the lake receded, and paleoshorelines are offset and no longer continuous. Twenty-four shoreline tufa samples were measured and calibrated, however 17 samples were eliminated, mostly due

to discordant duplicate ages and unacceptable $\delta^{13}\text{C}$ ranges. Results revealed Pluvial Lake Chewaucan's most recent highstand at $\sim 1,340$ m is 13.4 ± 0.1 to 13.7 ± 0.5 ka BP, with an average age of 13.5 ka BP, along with an earlier and higher highstand approximately 26.2 ± 0.2 to 34.3 ± 0.3 ka at $\sim 1,380$ m. Comparing fault scarp-based slip distribution data with four historical events, it is reasonable to estimate that there have been approximately three to six surface-rupturing events since the earlier higher highstand along the Winter Ridge and SMF segments, two to three events for the ARF segment since the most recent highstand, and one to two events on the TSF between 2.12-4 and 12-15 ka BP. The USGS estimated the WRF system to have a slip rate of 0.43 mm/yr. From this study, I presented slip rates that ranged between 0.18 to 0.74 mm/yr, which lie squarely in the middle of Crone et al (2009) published range. This method provided the opportunity for obtaining slip rates through means other than trenching.

ACKNOWLEDGMENTS

*I dedicate this thesis to those that fight invisible illnesses every day. Be strong, be brave,
and keep fighting!*

Fieldwork and geochronology was primarily funded by a National Earthquake Hazards and Reduction Program (NEHRP) of the USGS grant (G14AS00036) awarded to Dr. Anne Egger. Additional support for tuition, scholarships, and grants was awarded to J. Hall from Central Washington University Assistantships, the Geological Society of America's On To the Future Program, and the Yakima Rock and Mineral Club. Funding to collect samples in Summer Lake was provided by the National Earthquake Hazards Reduction Program (NEHRP) of the USGS, grant G14AS00036. I would like to thank GSA's On To the Future (OTF) program for providing travel funding and attendance to my first GSA meeting in 2016. I would like to thank the Yakima Rock Club for the scholarship and for being a warm and welcoming audience.

First, I would like to start by thanking Dr. Anne Egger for her support and guidance through this process. The door to Dr. Egger's office was always open whenever I needed help steering clear of the rabbit hole. As my teacher and mentor, she taught me more than I could ever give her credit for here. To her, I express my deepest gratitude.

I thank Dr. Lisa Ely and Dr. Walter Szeliga for providing critical feedback and serving on my committee. Your collective knowledge, constructive edits, enthusiasm, and support for my work and writing was instrumental and appreciated!

I would especially like to thank Daniel Ibarra, current Ph.D. Candidate at Stanford University. With his immense knowledge and instructive guidance, I am truly thankful to have had him as my mentor.

I would also like to thank and acknowledge Craig Scrivner and Moriah Kauer for being helpful, friendly, and extremely knowledgeable in just about everything. In my eyes-- Craig and Moriah comprise Central Washington University's very own "Dream Team" and any student would be and is lucky to be able to draw from their expertise!

To my many friends and family, you should know that your support and encouragement was worth more than I can express. Thank you for joining me in this journey!

Penultimately, I dearly express my very profound gratitude to my parents and to my partner, William Matsubu, for providing me with unfailing love and support, continuous encouragement throughout my years of study, and through the process of researching and writing this thesis. This accomplishment would not have been possible without you!

And finally, to my truest "rock" and bestest friend, though she can't possibly know just how truly happy and blessed she has made me, I'd like to thank my Marzy for her lifetime of love and support.

Thank you!

Jennifer Hall

TABLE OF CONTENTS

Chapter	Page
CHAPTER 1- INTRODUCTION.....	1
CHAPTER 2- BACKGROUND.....	6
Pluvial Setting.....	6
Tectonic Setting	11
Paleoseismology	13
Winter Rim Fault System	13
Slide Mountain Fault Segment	15
Winter Ridge Fault Segment	16
Ana River Fault Segment	16
Event I- ultimate earthquake	18
Event II- penultimate earthquake	19
Event III- the last sub- lacustrine earthquake	19
Event IV	20
Event V.....	20
Thousand Springs Fault.....	20
Relevant Historical Earthquakes	20
M _w 7.6 Pleasant Valley, NV Earthquake.....	23
M _s 7.2 Fairview Peak, NV- M _s 6.8 Dixie Valley, NV Earthquakes.....	23
M _s 7.5 Hebgen Lake, MT Earthquake.....	23
M _s 7.3 Borah Peak, ID Earthquake	24

TABLE OF CONTENTS (CONTINUED)

Chapter	Page
CHAPTER 3- METHODS.....	26
Radiocarbon Dating	26
LiDAR-Based Mapping.....	30
Calculating Offset	30
Calculating Slip Rates.....	32
CHAPTER 4- RESULTS.....	33
Radiocarbon Dating	33
Paleoshoreline Mapping.....	35
Fault Scarp Topographic Profiles and Surface Offset	38
CHAPTER 5- DISCUSSION	43
Comparing Fault Scarp-Based Slip Distribution Data with Historical Events	43
Slide Mountain Fault Segment	43
Winter Ridge Fault Segment	44
Ana River Fault Segment	45
Thousand Springs Fault.....	46
Comparing Fault Scarp-Based Slip Distribution with Local Events	47
Comparing Paleoshoreline-Based Surface Offsets with Local Events	48
Comparing Deformation with Catlow Valley.....	49
Paleoshoreline-Based Slip Rate Calculations	49
CHAPTER 6- CONCLUSION	55

TABLE OF CONTENTS (CONTINUED)

Chapter	Page
REFERENCES	57
APPENDIXES	62
Appendix A.....	62

LIST OF TABLES

Table	Page
1. Radiocarbon data from Lower Chewaucan Marsh and Lake Abert.	10
2. Fault segments within the Summer Lake Basin (Personius et al., 2003).....	12
3. Normal fault segmentations in the Basin and Range Province.....	21
4. Sample locations.	27
5. Radiocarbon ages for Summer Lake basin, from this study.	28
6. Percent differences between duplicate sample age ranges.	33
7. Paleoshoreline elevations and relative offsets.	49
8. Ten-Mile Ridge paleoshoreline highstand offset rate over ARF segment.....	51
9. Diablo Rim paleoshoreline highstand offset rate over ARF segment and TSF.....	51
10. Flatiron Point paleoshoreline highstand offset rate over ARF segment and TSF.....	51
11. Jacks Lake paleoshoreline highstand offset rate over WRF segment.....	51
12. Fremont Point paleoshoreline highstand offset rate over WRF segment.	52
13. Harvey Flat paleoshoreline highstand offset rate over WRF segment.	52
14. Hadley Butte paleoshoreline highstand offset rate over WRF segment.	52

LIST OF FIGURES

Figure	Page
1. Shaded-relief map of western United States showing Quaternary faults that have ruptured since 15 ka	2
2. Shaded-relief map of northwestern Basin and Range indicating location of active faults and locations of Pleistocene pluvial lakes.	3
3. Shaded-relief map of the Summer Lake basin located in south-central Oregon.	4
4. Annotated photo of paleoshorelines in the field	7
5. Annotated photo of capping tufa deposited on a prominent paleoshoreline located near Flatiron Point	8
6. A schematic figure of a normal fault scarp, Four topographic profiles of the WRF system	31
7. Calibrated radiocarbon ages plotted by elevation.	34
8. Prominent paleoshorelines from Pleistocene Pluvial Lake Chewaucan.	36
9. Surface offset from topographic profiles along the Winter Ridge fault segment.	39
10. Surface offset from topographic profiles along the Slide Mountain	39
11. Surface offset from topographic profiles along the Ana River fault segment	40
12. Surface offset from topographic profiles along the Thousand Springs fault.	40

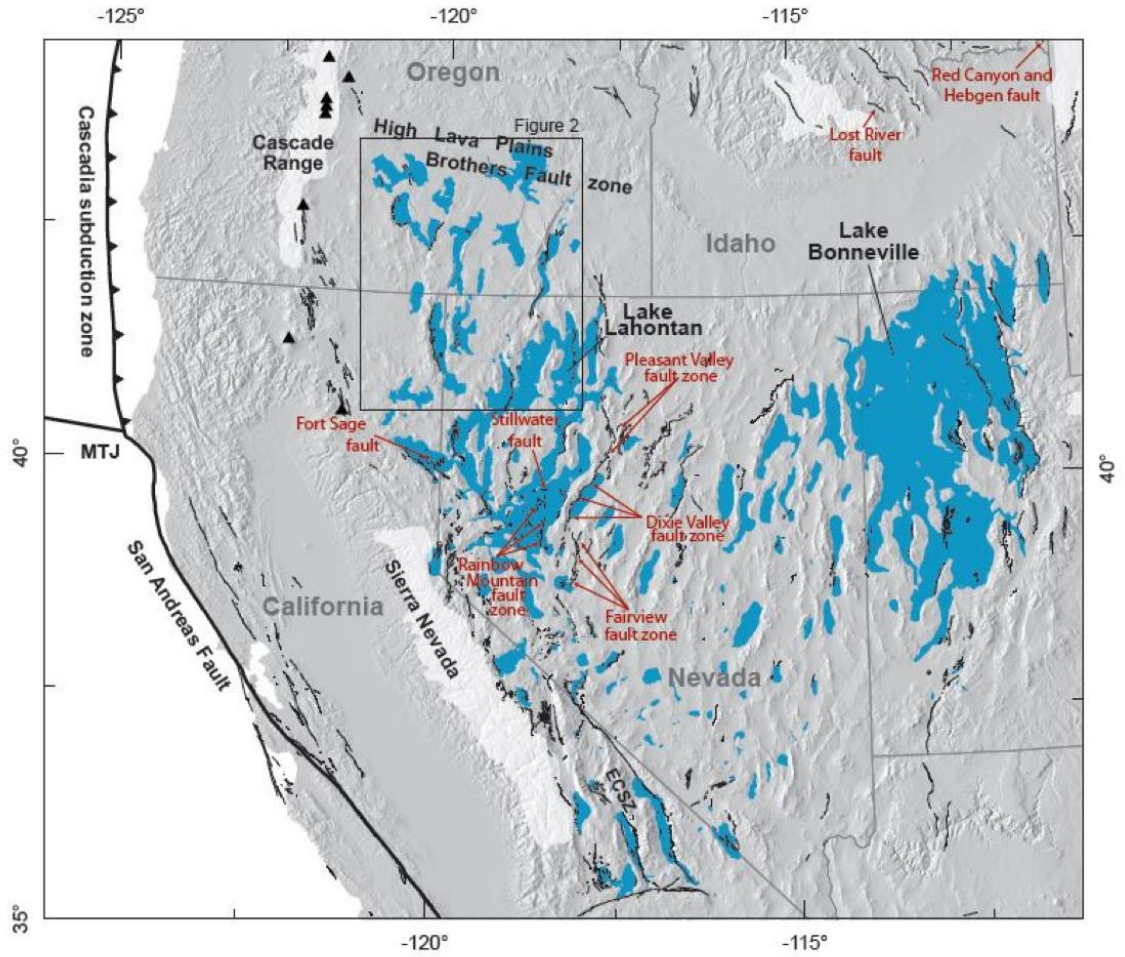
CHAPTER 1

INTRODUCTION

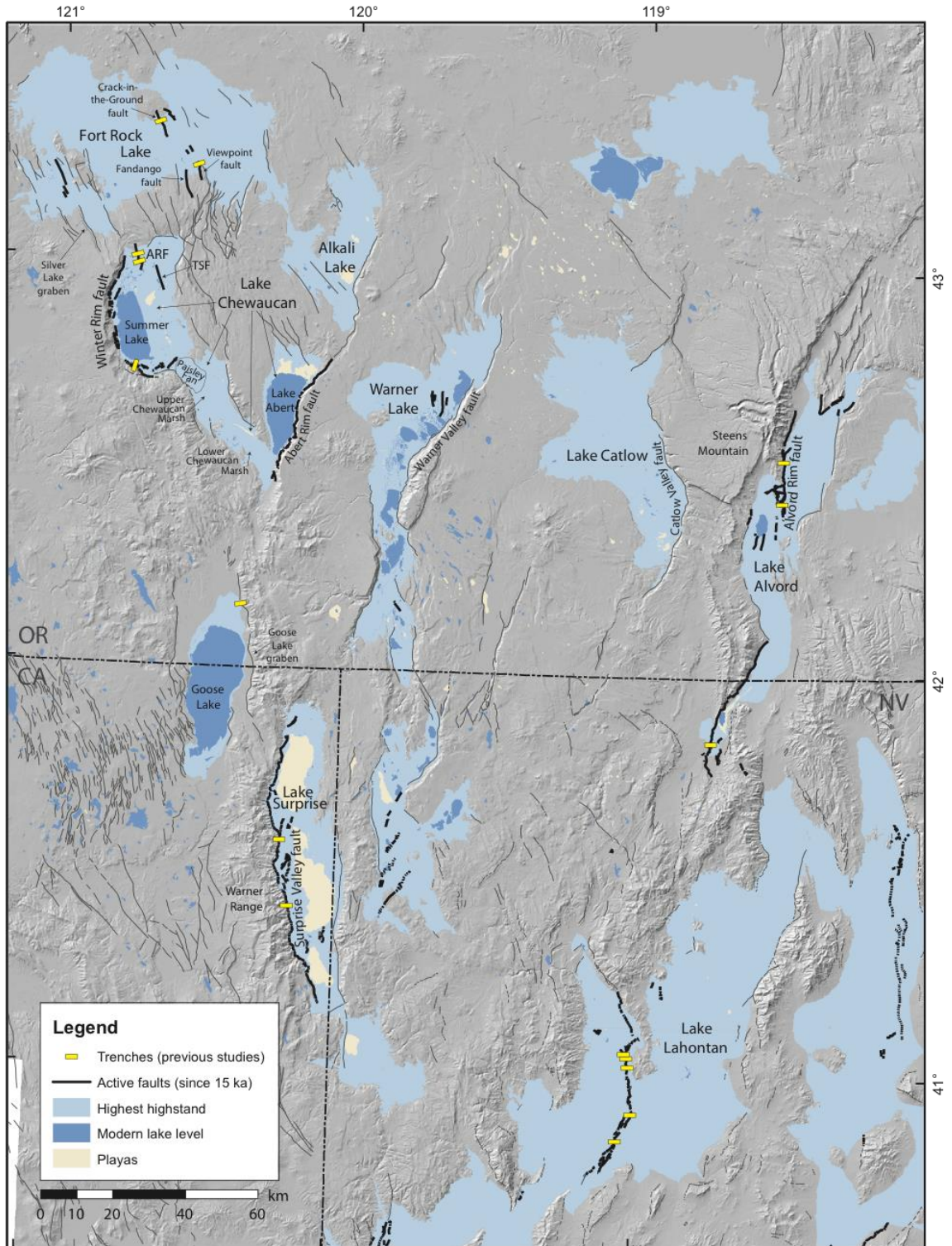
The northwestern Basin and Range (NWBR) is a region with active normal faults (**Error! Reference source not found.**) where earthquake recurrence intervals exceed seismicity records (Pezzopane and Weldon, 1993; Personius et al., 2009). Low modern strain rates (Kreemer et al., 2012) and lack of historical seismicity records for NWBR faults, including the Abert Rim fault, Alvord fault, Surprise Valley fault, and the Winter Rim Fault (WRF) system present a challenge to constraining the seismic hazard (**Error! Reference source not found.**) (Crone et al., 2009).

The WRF system, located along the northwestern edge of the NWBR (**Error! Reference source not found.**), encompasses several Holocene fault scarps that cut Quaternary sediments within the Summer Lake basin, suggesting an active system (Pezzopane, 1993). The USGS estimates that the 66-km long WRF system has a slip rate of 0.43 mm/yr, potential earthquake magnitudes of 6.5-7.19, and a recurrence interval of 3.1 thousand years (ky) (Crone et al., 2009). These estimates are based upon three trench investigations, two on the Ana River segment and one on the Slide Mountain segment (**Error! Reference source not found.** and **Error! Reference source not found.**). Trenching across the longest, largest-offset Winter Ridge segment has proven difficult because of high sedimentation rates associated with massive landslides that line the Winter Rim (Badger and Watters, 2004), yet this is the segment that is optimally oriented to slip in the current stress setting.

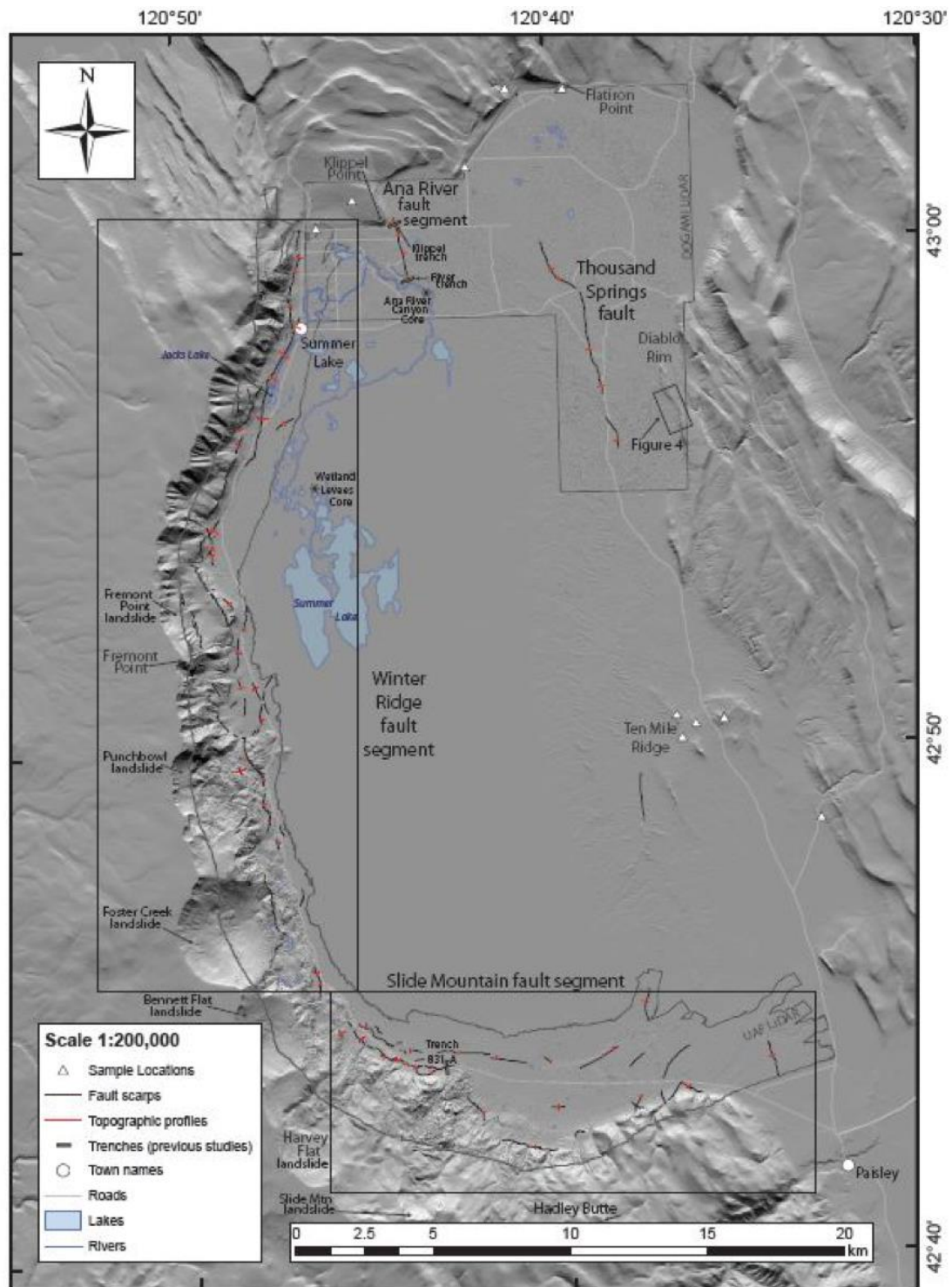
Fortunately, fault scarps cut a dateable geomorphic feature--tufa-coated paleoshorelines from Pleistocene Pluvial Lake Chewaucan. Because the faults have been



Error! Reference source not found.



Error! Reference source not found.



Error! Reference source not found.

active since the lake receded, these dateable, paleohorizontal features have been deformed, cut, and offset, and are no longer continuous.

By combining offset of paleoshorelines with radiocarbon dating of tufa and high-resolution Light Detection and Ranging (LiDAR)-derived elevation data, I am able to calculate surface offsets, dip slip rates, and slip distributions for the Winter Rim Fault system. With the lack of historical surface-rupturing events in the northwestern Basin and Range, datasets from this study will be compared with carefully selected, well-documented, normal-sense motion surface-rupturing events within 1,000 km of the Basin and Range. The historical events selected for this study, despite differences in tectonic settings, are ideal analogs for comparing historical slip distributions with slip distributions calculated for the WRF system.

These datasets allow us to address the question: How do surface offsets and slip rates vary spatially and temporally within the Summer Lake basin? This method has proven successful in nearby Surprise Valley, CA (Figure 2) (Marion, 2016) and the Alvord basin, OR (Figure 2) (Oldow and Singleton, 2008), providing an opportunity for obtaining dip slip rates through means other than trenching. The primary goal of this work is to quantify surface offsets and fault slip rates to better constrain hazard potential for the WRF system.

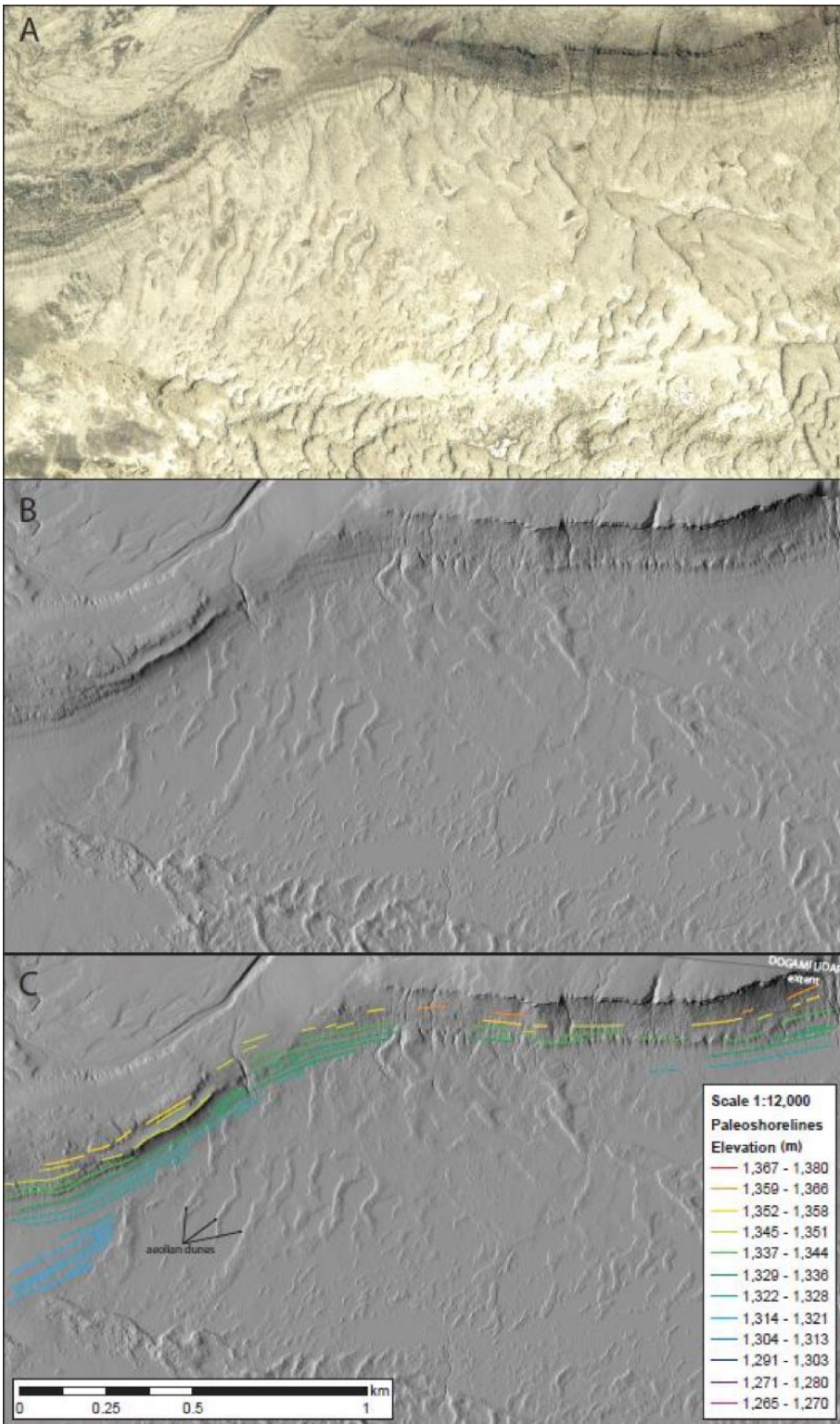
CHAPTER 2

BACKGROUND

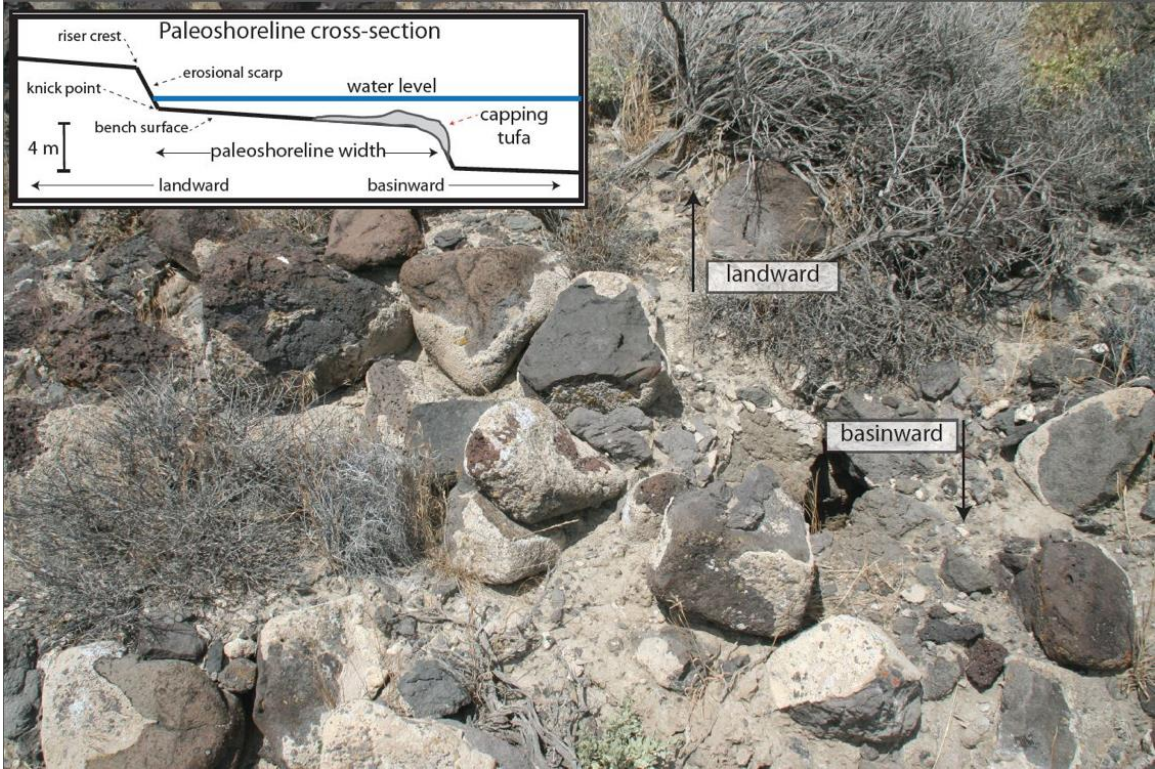
Pluvial Setting

The NWBR hosted several closed-basin pluvial lakes in the Pleistocene, including Lake Chewaucan (Figure 2), whose lake levels fluctuated due to changes in climate associated with the regression and transgression of the North American ice sheet. Lake Chewaucan had a maximum highstand (1,377 m, 113 m deep) approximately 1,314 thousand years ago (ka) before present (BP) (Cohen et al., 2000). Other significant highstands occurred ~200-165 ka BP and ~89-50 ka BP, as constrained by lithostratigraphic, paleontologic, and geochemical indicators within sediment cores (Cohen et al., 2000; Negrini et al., 2000).

Along the margins of the basin, paleoshorelines mark the highstands and stillstands (Figure 4). Paleoshorelines represent a paleohorizontal datum with a natural variability of about 2 m (Hopkins and Dawers, 2016). They can be either erosional or depositional features, and can take several forms, including wave-cut notches, beach ridges, berms, and bars. Controlling factors that dictate the type of feature that is formed include local slope, shoreline orientation, the amount and particle size distribution of sediment supply, accommodation space, wind strength, fetch, water depth, and the length of time that lake level remains stable at a particular elevation (Reheis et al., 2014). An erosional feature in one location, such as a wave-cut notch, may correlate with a depositional feature in another location, such as a beach ridge, berm, or bar, depending on depositional settings at given elevations and locations.



Error! Reference source not found.



Error! Reference source not found.

Tufa, a shore-zone lacustrine calcium carbonate (CaCO_3) deposit, can precipitate in the swash and photic zones in the form of capping tufa, beachrock, and capping tufa over beachrock (Figure 5) (Nelson et al., 2005; Felton et al., 2006). Tufa development correlates with bedrock exposure and landform orientation, as well as the longest fetch direction. As tufa deposits require wave agitation and biomediation to precipitate, these samples record lake level within a few meters (m) and can be radiometrically dated (Felton et al., 2006).

At Lake Chewaucan's maximum highstand of 1,377 m, the lake covered a surface area of 181 km^2 with a maximum depth of 113 m (Allison, 1982). Pluvial lakes can cause crustal flexure, as has demonstrated at Lake Bonneville and Lake Lahontan (Crittenden, 1963; Adams et al., 1999; Karow and Hampel, 2010; Hampel et al., 2010). In these cases, deformation of paleoshorelines is not caused only by slip along faults, but by isostatic rebound of the crust. Lake Bonneville had an average depth of 150 m, with a maximum depth of 335 m, and a surface area of $51,800 \text{ km}^2$ (Crittenden, 1963), and shorelines at the center of the lake were offset by a maximum of 35 m from those on the periphery. In comparing the volume of Lake Bonneville ($10,461 \text{ km}^3$) and Lake Lahontan ($2,054 \text{ km}^3$) (Karow and Hampel, 2010) to Lake Chewaucan ($\sim 20 \text{ km}^3$), the load exerted on the crust by Lake Chewaucan is $<1\%$ that of the large lakes, suggesting isostatic rebound is an unlikely factor in the Summer Lake basin. I therefore assume that the deviation of paleoshorelines from horizontal in the Summer Lake basin can be attributed to tectonic deformation.

Error! Reference source not found.

Table 1. Radiocarbon data from Lower Chewaucan Marsh and Lake Abert								
Shoreline Feature	Laboratory Number	Latitude (°N)	Longitude (°W)	Elevation (m)	¹⁴ C age (yr) ± 1σ	Calibrated age range (yr cal. BP) ±2σ	Median aged (yr cal BP)	Calibrated age (ka cal. BP) ±2σ IntCal13
Valvata humeralis	4F, AA13588	42.5129	120.3296	1335 ± 1	11930 ± 90	13560 - 14020	13760	13.79 ± 0.23
Valvata humeralis	6AV, AA13589	42.5990	120.1845	1310 ± 1	11670 ± 90	13320 - 13720	13500	13.52 ± 0.20
Vorticifex (Parapholyx) effusa	7EG, AA13590	42.5351	120.2280	1307 ± 1	11560 ± 120	13130 - 13610	13390	13.37 ± 0.24
Vorticifex (Parapholyx) effusa	7FG, AA13591	42.5351	120.2280	1310 ± 1	12030 ± 90	13710 - 14130	13890	13.92 ± 0.21

Radiocarbon data from Licciardi, 2001.

The overflow channel between Summer Lake and Upper Chewaucan Marsh (**Error! Reference source not found.**), across the Paisley fan, has an upper intake elevation of 1,336 m (Allison, 1982; Licciardi, 2001). However, groundwater flow in permeable sediments and fault zones may allow the water level to equilibrate across the four sub-basins (Langridge et al., 2001). Licciardi (2001) reported radiocarbon ages of gastropods (**Error! Reference source not found.**), three of which located in latest Pleistocene shorelines at Lake Abert, and the other in the fan-delta in Lower Chewaucan Marsh (**Error! Reference source not found.**). Although helpful constructing paleolake levels, the Lake Abert radiocarbon ages are not useful for calculating slip rates in the Summer Lake basin. The land barrier between the two water basins will still allow the basins to be connected, but that does not necessarily mean that they will equilibrate at the same elevation. Comparing elevations of paleoshoreline tufas of both basins would not yield useful data because there are many faults in between Summer Lake and Lake Abert. Due to these variables, only radiocarbon ages from the Summer Lake basin will be used in this study.

Tectonic Setting

The northwestern Basin and Range (NWBR) lies north of the Mendocino triple junction (MTJ), inboard of the active Cascadia subduction zone (**Error! Reference source not found.**). Much of the strain that passes inboard and north of the MTJ may not be accommodated by rigid fault blocks, but by structures near the convergent boundary (Pezzopane, 1993). The stress regime changes from compression in the subduction setting on the coast to extension in the Basin and Range Province. The Winter Rim fault system bounds the Summer Lake basin in south-central Oregon (**Error! Reference source not found.**). Other fault systems within the NWBR include the Surprise Valley, Goose Lake Graben, Warner Valley, Abert Rim, Viewpoint, and Crack-in-the-Ground (**Error! Reference source not found.**).

Regional principal stress directions were determined by Crider (2001) analyzing 23 $M_w > 4.0$ earthquake focal mechanisms for the past 90 years between the Brother's fault zone and the Cascade volcanic arc (**Error! Reference source not found.**). With this method, the least compressive stress, or direction of extension, was determined to be oriented nearly E-W (264°). Crider (2001) also noted dikes that strike ENE-WSW (256°), alignments of three of more cinder cones that trend N-W (244°), and NS alignment of joints in lacustrine sediments that compared favorably to regional stress inversions. Treerotchananon (2009) analyzed the magnitude of extension in all horizontal directions for 161 fault scarps and 56 fault blocks on the north end of the Summer Lake basin (**Error! Reference source not found.**) resulting in an estimated extension of 1.5–5.5% along the maximum extension direction of 285° . Pezzopane and Weldon (1993)

characterized regional fault orientations to estimate a horizontal slip azimuth of 267° .

From this, I infer a regional extension direction that is

Error! Reference source not found.

Fault segment	Average azimuth	Length (km)	Dip direction
Winter Ridge	356°	29.5	E
Slide Mountain	300°	16.1	NE
Ana River	345°	7.5	E
Thousand Springs	175°	8.1	W

E-W to slightly ENE-WNW in the Summer Lake region (Crider, 2001; Treerotchananon, 2009; Pezzopane and Weldon, 1993).

The Winter Rim fault (WRF) system cuts Tertiary basalt flows and basaltic cinders dated at 6.3 ± 0.4 Ma and 6.6 ± 0.3 Ma, respectively (Diggles et al., 1990). Therefore, slip along the faults that formed the Summer Lake basin initiated $<6.3 \pm 0.4$ Ma.

The WRF system is a normal fault divided into three segments: Slide Mountain, Winter Ridge, and Ana River (**Error! Reference source not found.**). The west-dipping Thousand Springs fault (TSF) also lies within the Summer Lake basin (**Error! Reference source not found.**). The Summer Lake basin is a half-graben, with the major basin-bounding structure of the Winter Ridge fault to the west and Slide Mountain fault to the south (**Error! Reference source not found.**). The Winter Ridge section is the longest section of the fault system, displays the largest fault scarps, and is most favorably oriented to slip in the current stress field (**Error! Reference source not found.**). While paleoseismic studies have been conducted on the Ana River Fault, the fault length is relatively minor compared to Winter Ridge fault section that has not had paleoseismic studies. Fault scarp heights vary from less than 1 m to composite scarps more than 750

m; simple relationships between scarp height and scarp length have not yet been identified (Crider, 2001).

There are disputes on whether the Ana River fault (ARF) is a splay or segment of the WRF, or a separate fault. Pezzopane (1993) argued that the ARF may connect or be a splay of the WRF system due to the large amount of displacement for a fault of short length. Langridge (1998) suggests that instead of a splay for the WRF system, the ARF is a short fault that is involved with a complex stepover from the Summer Lake graben to the Silver Lake graben (**Error! Reference source not found.**). Another hypothesis is that the ARF is involved in a series of right-stepping active normal faults that trend towards Fandango and Viewpoint faults in the north (**Error! Reference source not found.**) (Langridge, 1998). Utilizing equations from Wells and Coppersmith (1994), if the ARF has approximately 2-4 m of surface offset, then the scaling relations of the fault length predict a length of approximately 34-45 km (Langridge, 1998). For the purposes of this study, the Ana River fault is considered a segment of the WRF system because it lies 1.5 km away from the Winter Ridge fault.

Paleoseismology

A number of previous studies have investigated the paleoseismicity of the Winter Rim Fault system. I provide a brief overview of these studies here in order to provide comparison for my results.

Winter Rim Fault System

The topographic rims surrounding the Winter Ridge and Slide Mountain fault segments are Miocene to early Pliocene basalt flows that lay nearly horizontal (Travis,

1977; Walker, 1963). Discontinuously beneath the basalt rim, the Miocene to early Pliocene rhyolitic and dacitic tuff, tuffaceous sedimentary rocks, and rhyodactitic and andesitic flows dip 5° to 10° westward into the escarpment (Walker, 1963).

Badgers and Watters (2004) analyzed three of the seven major landslides in the Summer Lake basin (**Error! Reference source not found.**) and the maximum to minimum ages determined were the following: 1) Bennett Flat: 900-270 to 16.8 ka BP; 2) Foster Creek: 180 to 16.8 ka BP; and The Punchbowl: 10 to 1.9-4 ka BP. Negrini and Davis (1991) used a correlation model with projecting the stratigraphic position of geologic features of the relatively poorly dated Summer Lake record with the relatively well-dated pluvial Lake Russell (modern-day Mono Lake) in eastern California, predicting a maximum age of 16.8 ka BP for the end of the Pleistocene pluvial Lake Chewaucan highstand. The 16.8 ka BP highstand age is based on a superimposed paleoshoreline on the Bennett Flat landslide debris at an elevation of 1,378 m and the stratigraphic position of the youngest lacustrine sediments a few cm above Tephra A (Badger and Watters, 2004). However, within the LiDAR-based mapping, I do not see evidence of a paleoshoreline superimposed on the Bennett Flat landslide at the elevation of 1,378 m.

Badger and Watters (2004) estimate that the Winter Ridge-Slide Mountain fault segments is capable of producing a $M_w \approx 7$ earthquake, the basis of landslides that line the western-southwestern margin of the basin. Pseudostatic analysis revealed that strong shaking was required to initiate landsliding events, triggering the weak tuffaceous east-dipping sedimentary rocks to fail along planar surfaces and the overlying 1-km thick

volcanic basalt flow sequence to landslide. (Badger and Watters, 2004). Landslide debris is mostly unstratified mixtures of basaltic and tuffaceous sedimentary bedrock.

Slide Mountain Fault Segment

The Slide Mountain fault segment of the WRF system is located on the southern boundary of the basin (**Error! Reference source not found.**) and dips to the northeast with a strike of 300° (**Error! Reference source not found.**), highly oblique to the current E-W extension direction. Pezzopane (1993) conducted two trench investigations along the Slide Mountain segment (trenches 831a-1, 831a-2) (**Error! Reference source not found.**), while only one trench (831a-1) was logged and described.

These trenches exposed a fault zone in Pleistocene pluvial deposits, fluvial and reworked alluvial deposits, debris flows, and colluvium (Pezzopane, 1993). The lowermost deposits in the downthrown block were intensely folded, faulted, and interlayered with fault-derived colluvium (Pezzopane, 1993), suggesting multiple events that occurred while Lake Chewaucan stood at a level above the trench. Lacustrine units have wavy and irregular contacts with adjacent units, likely the result of coseismic soft-sediment deformation (Pezzopane, 1993).

Immediately east of Trench 831a-1 (**Error! Reference source not found.**), a stream cut alluvial fan deposit consisted of landslide debris, reworked alluvium, and burn layers with an abundance of charcoal (Pezzopane, 1993). A recalibrated radiocarbon age of 2.12 ± 0.21 ka BP on the charcoal provides a minimum age for the faulting (Pezzopane, 1993). The lower portion of this landslide deposit is cut by the 2-4 ka BP Neopluvial paleoshoreline at an elevation of 1,280 m (Allison, 1982).

Near Trench 831a-2 (**Error! Reference source not found.**), a piece of charcoal was buried 4-5 m beneath the surface of lacustrine section of the footwall block at an

elevation of approximately 1,341 m (Pezzopane, 1993). A recalibrated radiocarbon age of 38.5 ± 1.6 ka BP (Pezzopane, 1993). provides an age for these deeper shoreline deposits.

For the Slide Mountain fault segment, Pezzopane and Weldon (1993) determined an estimated average slip rate of 0.4-0.6 mm/yr from vertical offsets along three topographic profiles across the scarp and an estimated age of displaced lacustrine sediments and colluvium of approximately 16 ka BP.

Winter Ridge Fault Segment

There have been no paleoseismic trenching studies along the Winter Ridge fault segment of the Winter Rim Fault system (**Error! Reference source not found.**). The lack of trenching may be because of the high sedimentation rates from the surrounding km-high bedrock escarpment and landslide debris, making it difficult to quantify vertical offset due to the absence of correlative lakebed units on either side of the fault. On the basis of large landslide deposits, Badger and Watters (2004) estimated that the Winter Ridge-Slide Mountain fault is capable of producing M_w 7 earthquakes. In addition, long-term Miocene vertical slip rates of 0.3-0.44 mm/yr and >0.4 mm/yr were calculated for the Winter Ridge section by Simpson (1990) and Langridge (1998), respectively, based on the age of 6.3-6.6 Ma for the rim-capping basalts (Diggles et al., 1990), and sediment-filled depth of 1.5 km (Langridge, 1998).

Ana River Fault Segment

The Ana River fault segment, located in the northern region of the Summer Lake basin (**Error! Reference source not found.**), dips to the east with a strike of 345°

(**Error! Reference source not found.**). Of the three Winter Rim Fault system segments, the most paleoseismic studies were conducted on the Ana River fault, which has one of the best preserved tephrostratigraphic records in the northwestern United States (Langridge et al., 2001).

Pezzopane and Weldon (1993) logged a trench at the southern end of Klippel Point (**Error! Reference source not found.**) that revealed Pleistocene tephra layers displaced by approximately 4 m by at least two surface-rupturing earthquakes. Younger faults cut older fault-derived colluvial wedges, which lie unconformably on well-bedded lacustrine sands, leading Pezzopane (1993) to infer that this event occurred soon after the deposition of the lacustrine sands and the uppermost tephra. Based on the stratigraphic position of the tephra and the relative position of the four dated ashes, Pezzopane (1993) inferred that the two youngest faulting events occurred after the withdrawal of Pleistocene Lake Chewaucan, which he estimated was 16 ka BP.

The trench exposed a broad deformation zone, but a relatively narrow fault zone in the beveled and deformed pluvial lake deposits, that occurred while pluvial Lake Chewaucan stood above the trench site (Pezzopane and Weldon, 1993). Using an offset of 5 m, which Pezzopane (1993) interpreted as evidence for earlier episodes of faulting prior to the lake withdrawal, the Ana River fault segment has a slip rate of approximately 0.3 mm/yr. Pezzopane and Weldon (1993) measured displacement on four topographic profiles along Ana River Fault with an average surface offset of 3.25 m, while projecting far-field slopes indicated overall vertical separation of ~4 m. The slip rate is estimated to be approximately 0.2-0.6 mm/yr (Pezzopane and Weldon, 1993).

Langridge (1998) describes evidence for surface-rupturing events through a series of outcrop exposures and trench excavations near the River Trench, located on the southern bank of the Ana River (**Error! Reference source not found.**). By calculating sedimentation rates and correlating tephra from trench and natural exposures, Langridge (1998) determined the ages of eleven middle-to-late Quaternary faulting events that he assigned to the Ana River section: 47.6 ka BP, 7.6-14 ka BP, 12-15 ka BP, 25.5 ± 1.0 ka BP, 27-31 ka BP, 51 ± 5 ka BP, 73 ± 7 ka BP, 81 ± 6 ka BP, 130 ± 5 ka BP, 160 ± 10 ka BP, and 167 ± 10 ka BP. Overall, a complete record of eight events are recognized over the past ~87 ky with additional older, less-constrained events before this time. The average recurrence interval over these eight events is ~11 ky with a slip rate of ~0.12--0.14 mm/yr (Langridge, 1998). The five most recent events described by Langridge (1998) span the Holocene to early Quaternary timeline most applicable to this study with correlating the radiocarbon ages of the paleoshoreline tufa. These events are further described below.

Event I- ultimate earthquake

Pezzopane (1993) inferred that the 4-m fault scarp formed during two post-lake events. As the Ana River scarp does not extend and continue to be prominent beyond the 1,280-m elevation “Neopluvial” shoreline (Allison, 1982), Langridge (1998) reasons that the event occurs before the re-advancement of Winter Lake, which later eroded the scarp farther downbasin. The event also occurs before the re-development of aeolian dunes. Within the River Trench, there are several vertical fissures filled with Mazama Tephra that do not cut the overlying Mazama dune deposits (Langridge, 1998). Therefore, Event I is bracketed between after the Mazama eruption of ~7.6 ka BP and before the Winter

Lake advancement ~4 ka BP. The “Neopluvial” shoreline cuts an alluvial fan deposit near Slide Mountain fault segment; at the base of the deposit a radiocarbon date of 2.12 ± 0.21 ka BP from pieces of charcoal provide a minimum age of faulting. Therefore, Event I may have occurred between 7.6 ka BP and 2.12-4 ka BP.

Event II- penultimate earthquake

Due to the large amount of offset in the fault scarps post-lake and the absence of Mazama tephra, another event must have occurred pre-Mazama eruption (~7.6 ka) and after the lake receded. Within the strata, there are brittle fractures in the form of fissures, which imply water levels had dropped below the levels of both trenches by time of Event II. Langridge (1998) suggests that Lake Chewaucan fluctuated from moderate to higher water levels ~10 ka, indicating a maximum age of faulting. Therefore, Event II may have occurred between 7.6 and 10 ka BP.

Event III- the last sub-lacustrine earthquake

This event post-dates all known tephra ages and is associated with soft sediment deformation. The upper most lacustrine silts and coarse-grained gravel facies at Klippel Trench are offset, which is consistent with the known water levels around Klippel Point at that time (Langridge, 1998). Fault traces cut and postdate the entire deep-water Ana River section (Negrini et al., 2000; Cohen et al., 2000), which is overlain by shallow water deposits. Based on the rate of sedimentation, the surface of the deep-water deposits is estimated to be around 14 ka (Langridge, 1998). There has been no observation of the 4 Craters Tephra, age dated to 13 ± 1 ka, within this section of strata (Langridge, 1998). Between the age inferences of the drying lake and the youngest lake-deposited tephra, this event may have occurred between 12 and 15 ka (Langridge, 1998).

Event IV

The angular and onlap relations between the Trego Hot Springs Tephra and Wono Tephra, along with the thickened section adjacent between the two tephra, point to being evidence for Event IV. This event is constrained below Tephra E and an evaporitic unit above, occurring approximately 25.5 ± 1.0 ka (Langridge, 1998).

Event V

Evidence for Event V is mainly stratigraphic, by the increased offset, onlap, and gentle lacustrine folding sequence of the Trego Hot Springs Tephra and Wono Tephra (Langridge, 1998). This event is constrained below Tephra G with the Wono Tephra above, occurring approximately 27-31 ka (Langridge, 1998).

Langridge (1998) describes six more events in detail, lumping them into a category of older events.

Thousand Springs Fault

There have been no paleoseismic studies along the Thousand Springs fault (**Error! Reference source not found.**). The west-dipping Thousand Springs fault is located on the central-eastern portion of the basin, among sand dunes and Miocene to Pliocene intrusive rhyolitic and dacite plugs, dikes, and complex domes, including related flows and flow breccia (Walker, 1963).

Relevant Historical Earthquakes

Although paleoseismicity studies show that the region is seismically active, there have not been any historical surface-rupturing earthquakes in the WRF system or even

within the northwestern Basin and Range (**Error! Reference source not found.**). In order to determine if the slip

Error! Reference source not found.

Table 3. Fault segmentation in Basin and Range Province normal faults

No.	Date†	Magnitude†	Earthquake or structural fault segment	Surface rupture length (km) (end-to-end)†	Avg displacement (m)
1	10/03/15	$M_w = 7.6$	Pleasant Valley, NV	60	2.00†
			China Mtn fault segment	10	0.90*
			Tobin fault segment	8.5	1.90*
			Pearce fault segment	30	2.80*
			Sou Hills fault segment	10.5	0.90*
2	12/14/50	$M_L = 5.6$	Fort Sage Mtn, CA	9.5	0.16 γ
3	07/06/54	$M_s = 6.3$	Rainbow Mtn, NV	18	0.22 β
4	08/24/54	$M_s = 7$	Stillwater, NV	59.5	0.22 β
			Rainbow Mtn segment	53	0.22 β
			Fourmile Flat segment	6.5	0.22 β
5	12/16/54	$M_s = 7.2$	Fairview Peak, NV	67	1.20 ϕ
			Fairview fault segment	32	1.20 ϕ
			Westgate fault segment	18	0.40 ϕ
			Gold King fault segment	16	0.45 ϕ
6	12/16/54	$M_s = 6.8$	Dixie Valley, NV	43-47	0.90 ϕ
7	08/17/59	$M_s = 7.5$	Hebgen Lake, MT	28	2.36 κ
			Red Canyon fault segment	23	2.57 κ
			Hebgen fault segment	12	1.97 κ
8	10/29/83	$M_s = 7.3$	Borah Peak, ID Lost River fault	36	1.82 κ
			Warm Springs fault segment	14	1.40 κ
			Thousand Springs fault segment	21	2.10 κ

M_w = moment magnitude, M_L = local magnitude, M_s = surface-wave magnitude
†(DePolo et al. 1991) *(Wallace, 1984) γ (Briggs, 2013) β (Caskey, 2004) ϕ (Caskey, 1996) κ (Barrientos, 1987)

distributions calculated in this study are reasonable, I must compare them to historical surface-rupturing events. By utilizing the correlative relationship between earthquake rupture parameters, such as fault length and displacement, and earthquake magnitudes as outlined by Wells and Coppersmith (1994), I can compare my dataset with well-documented historical events. Badgers and Watters (2004) estimated the Winter Ridge-Slide Mountain fault segments capable of producing a $M_w \approx 7$ earthquake.

To find possible historical analogues for this study, I am extending the physical boundaries outside of the NWBR. As of 2017, there have been 13 historical surface-rupturing earthquakes in the Basin and Range Province (DePolo et al., 1991; U.S. Geological Survey Earthquake Hazards Program, 2017). These events have a wide range of variability in their surface-rupturing patterns, as the Basin and Range is deforming spatially and temporally at different rates (DePolo et al., 1991; U.S. Geological Survey Earthquake Hazards Program, 2017). By eliminating historical events outside of 1,000 km from the WRF system and those with strike slip senses of displacement, there are eight historical events to consider when comparing historical slip distributions with slip distributions calculated for the Winter Rim fault system (**Error! Reference source not found.**).

Normal fault data from eight historical events were considered to be analogues in this study. I compared surface rupture lengths and average displacements, along with comparing earthquake magnitudes for those that have been recorded (**Error! Reference source not found.**). Upon further research, I eliminated three additional historical earthquakes from this study. The M 5.6 Fort Sage earthquake was eliminated when compared to WRF earthquake magnitude estimations (6.5-7.19) (Crone et al., 2009). Rainbow Mountain and Stillwater earthquakes was eliminated from the study because the amount of right-lateral offset recorded was greater than the vertical separation, and this study is based on normal-slip faults (Caskey et al., 1996). Pleasant Valley, Dixie Valley/Fairview Peak, Hebgen Lake, and Borah Peak fault scarps are all excellent analogues to compare slip distribution data of historical earthquakes to slip distribution recorded in the fault scarps of the Summer Lake basin. They are well-documented, have

similar fault lengths, and the majority of them ruptured in multiple segments. Despite somewhat differences in tectonic setting within the Basin and Range, these five historical earthquake events are useful analogues for comparing slip distribution data.

M_w 7.6 Pleasant Valley, NV Earthquake

On October 2, 1915, four main scarps developed in a right-stepping en echelon pattern during a surface-rupturing event with a 60-km long rupture length (**Error! Reference source not found.**). From northeast to southwest, the fault segment rupture lengths were: China Mountain (10-km length); Tobin (8.5-km length); Pearce (30-km length); and Sou Hills (10.5-km length). The average vertical displacement was 2 m and the maximum displacement of 5.8 m occurred on the Pearce scarp (Wallace et al., 1984). The scarps are thought to have been well preserved because of the desert climate of the region.

M_s 7.2 Fairview Peak, NV- M_s 6.8 Dixie Valley, NV Earthquakes

On December 16, 1954, the M_s 7.2 Fairview Peak earthquake produced a 32-km rupture with right-oblique slip where the right-lateral and vertical separation reached a maximum 2.9 and 3.8 m, respectively, and an average vertical displacement of 1.2 m (**Error! Reference source not found.** and **Error! Reference source not found.**) (Caskey et al., 1996). A subsequent event, the Dixie Valley M_s 6.8, had a normal slip sense with a maximum vertical separation of 2.8 m, and an average vertical displacement 0.9 m (**Error! Reference source not found.** and **Error! Reference source not found.**)

(Caskey et al., 1996). Surface ruptures attributed to the Dixie Valley earthquake were limited to the Dixie Valley fault.

M_s 7.5 Hebgen Lake, MT Earthquake

On August 17, 1959, the M_s 7.5 Hebgen Lake earthquake struck the 28-km long en-echelon Hebgen and Red Canyon faults (**Error! Reference source not found.**). The fault dips 45° to 50° and extends to depths of 10 to 15 km (Barrientos et al., 1987). Average displacement for entire rupture length was 2.36 m (**Error! Reference source not found.**).

M_s 7.3 Borah Peak, ID Earthquake

On October 28, 1983, the Borah Peak earthquake (M_s 7.3) occurred on the Lost River Range fault in east-central Idaho (**Error! Reference source not found.**). The 36-km long fault is divided into three sections: a) 21-km-long Thousand Springs southern segment, b) a 14-km-long Warm Springs western segment, and c) an 8.2-km-long northernmost segment (Crone et al., 1984; Scott et al., 1985). The average vertical displacement measured was 1.82 m along the entire surface rupture (**Error! Reference source not found.**).

The Thousand Springs segment of the Lost River fault has the largest amount of throw, highest scarps, evidence of sinistral slip, and the most complex features (Crone et al., 1984; Crone and Haller, 1991). The average displacement for the Thousand Springs segment was 2.1 m, and the largest vertical displacement was approximately 4 m (**Error! Reference source not found.**) (Crone et al., 1984). The complexity and net throw on

scarps vary considerably, and in many places en echelon scarps indicate both synthetic and antithetic displacements (Crone et al., 1984).

Surface rupture along the 14.6-km long Warm Springs western segment is separated from the Thousand Springs fault segment by a 4.7 km gap. The average vertical displacement for the Warm Springs segment was 1.4 m (**Error! Reference source not found.**). The northernmost segment has a maximum throw of 1 m (Crone et al., 1984). Slip rates for the Lost River Range fault have been estimated to be 1 mm/yr with the overall region accommodating east-west extension (Scott et al., 1985).

While the Winter Rim fault system encompasses several Holocene fault scarps, there have been no recent surface-rupturing events. By carefully investigating surface offsets of fault scarps and shoreline offsets, I can compare the slip distributions of the Winter Rim fault segments to those that have been well-documented to better constrain the seismic history of the WRF system, and thus provide input to the seismic hazard potential of the region.

CHAPTER 3

METHODS

Radiocarbon Dating

Eighteen carbonaceous shoreline tufa samples spanning elevations from 1,316 m to 1,406 m were collected in the field in August 2015 (Table 4). Tufa was collected from locations where dense frameworks of capping tufa with minimal vesicles were laterally continuous along wave-formed shorelines (Figure 4, Figure 5, and Plate I); suitable locations were limited to the northern and eastern portions of the basin. Seventeen samples were carbonaceous tufas and one was a carbonaceous shell, 15 lie east of the Thousand Springs fault, two lie west of the Ana River fault, and two lie between the Ana River and Thousand Springs faults (Figure 3). Elevation of the tufa samples, extracted from either the 10-m (± 2.0 m) DEM or the 1-m (± 0.1 m) high-resolution LiDAR, is based on the latitude and longitude of the sample location collected with a handheld GPS unit. All samples were dated using accelerator mass spectrometry (AMS) radiocarbon geochronology; duplicates of six of the 18 samples were also analyzed (Table 5).

To prepare the tufa samples for radiocarbon dating, they were cleansed with ethanol to minimize possible contamination. To carve and obtain 30 mg of dense tufa carbonate, I used a Dremel with a diamond-wheel rotary saw. The Dremel and diamond-wheel rotary saw were cleansed with ethanol between each dense tufa carbonate sample. The samples were placed in plastic bags, labeled, and sent to Direct AMS, a geochronological analysis laboratory in Bothell, WA, where they were analyzed according to their standard procedures.

Error! Reference source not found.

Table 4. Sample locations			
Sample name	Latitude (°N)	Longitude (°W)	Elevation (m)
SL15AE02	42.80892	120.55169	1383.3 ± 2.0
SL15AE03	42.80836	120.55128	1383.0 ± 2.0
SL15AE04*	43.05045	120.68407	1381.2 ± 2.0
SL15AE05*	43.05017	120.65868	1343.7 ± 2.0
SL15AE06	43.05006	120.65854	1341.3 ± 2.0
SL15AE07	42.83618	120.61262	1355.4 ± 2.0
SL15AE08	42.84355	120.61484	1342.6 ± 2.0
SL15AE09	42.84078	120.60642	1350.9 ± 2.0
SL15JH01	42.80892	120.55169	1383.2 ± 2.0
SL15JH03	43.01487	120.75370	1393.6 ± 0.1
SL15JH04	43.04990	120.65894	1329.1 ± 0.1
SL15JH05	43.04992	120.65921	1328.3 ± 0.1
SL15JH06*	43.04984	120.65928	1324.9 ± 0.1
SL15JH07*	42.84211	120.59363	1407.0 ± 2.0
SL15JH08	42.84228	120.59378	1405.5 ± 2.0
SLT1-2C-1*	43.02515	120.70330	1344.5 ± 2.0
SLT3-1B	43.00600	120.77000	1316.8 ± 0.1
SL15BM01	42.80870	120.55151	1383.2 ± 2.0
SL15BM02	43.04979	120.65844	1328.3 ± 0.1
SL15BM03	43.05001	120.65847	1342.0 ± 2.0
SL15BM04*	42.84256	120.59393	1402.1 ± 2.0
Samples in bold were selected for radiocarbon dating.			
*Samples with duplicate sampling			

Error! Reference source not found.

Table 5. Radiocarbon ages for Summer Lake									
Sample Name	Laboratory Number	Latitude (°N)	Longitude (°W)	Elevation (m)	$\delta^{13}\text{C}$	^{14}C age (yr) $\pm 1\sigma$	Calibrated age range (yr cal. BP) $\pm 2\sigma$	Median aged (yr cal BP)	Calibrated age (ka cal. BP) $\pm 2\sigma$ IntCal13
SL15AE02	D-AMS 013002	42.80892	120.55169	1383.3 \pm 2.0	1.4	21918 \pm 91	25917 - 26382	26118	26.15 \pm 0.23
SL15AE07	D-AMS 16778	42.83618	120.61262	1355.4 \pm 2.0	-2.8	36578 \pm 214	40705 - 41674	41225	41.19 \pm 0.48
SL15AE06	D-AMS 013005	43.05006	120.65854	1341.3 \pm 2.0	1.9	11565 \pm 44	13296 - 13477	13399	13.39 \pm 0.09
SL15JH01	D-AMS 013011	42.80892	120.55169	1383.2 \pm 2.0	-1.9	30271 \pm 136	33975 - 34605	34281	34.29 \pm 0.32
SL15JH05	D-AMS 013013	43.04992	120.65921	1328.3 \pm 0.1	0.2	11873 \pm 42	13572 - 13770	13676	13.67 \pm 0.10
SL15AE04	D-AMS 013003	43.05045	120.68407	1381.2 \pm 2.0	-3.8	25859 \pm 114	29643 - 30534	30089	30.09 \pm 0.45
SL15AE04_R	D-AMS 16784	43.05045	120.68407	1381.2 \pm 2.0	-1.6	25291 \pm 82	29053 - 29617	29348	29.34 \pm 0.28
Excluded due to $\delta^{13}\text{C}$ ranges									
SL15AE05	D-AMS 013004	43.05017	120.65868	1343.7 \pm 2.0	5.7	12487 \pm 49	14298 - 15034	14695	14.67 \pm 0.37
SL15AE08	D-AMS 013006	42.84355	120.61484	1342.6 \pm 2.0	4.3	10983 \pm 38	12729 - 12974	12828	12.85 \pm 0.12
SLT1-2C-1	D-AMS 013009	43.02515	120.70330	1344.5 \pm 2.0	5.0	12476 \pm 42	14288 - 14998	14663	14.64 \pm 0.36
SL15JH03	D-AMS 013012	43.01487	120.75370	1393.6 \pm 0.1	-6.9	30486 \pm 143	34124 - 34766	34456	34.45 \pm 0.32
SL15AE09_R	D-AMS 16788	42.84078	120.60642	1350.9 \pm 2.0	8.0	43390 \pm 321	45806 - 47372	46538	46.59 \pm 0.78
SL15JH08	D-AMS 16781	42.84228	120.59378	1405.5 \pm 2.0	3.9	19480 \pm 53	23184 - 23689	23473	23.44 \pm 0.25
SL15JH04	D-AMS 16779	43.04990	120.65894	1329.1 \pm 0.1	8.3	12310 \pm 37	14074 - 14541	14240	14.31 \pm 0.23
SL15BM03	D-AMS 16780	43.05001	120.65847	1342.0 \pm 2.0	7.2	12041 \pm 35	13763 - 14020	13883	13.89 \pm 0.13
Excluded due to lack of overlap in duplicates									
SL15JH06	D-AMS 013014	43.04984	120.65928	1324.9 \pm 0.1	-1.8	22152 \pm 76	26105 - 26621	26352	26.36 \pm 0.26
SL15JH06_R	D-AMS 16783	43.04984	120.65928	1324.9 \pm 0.1	0.1	25655 \pm 80	29466 - 30204	29787	29.84 \pm 0.37
SL15BM04	D-AMS 013008	42.84256	120.59393	1402.1 \pm 2.0	-2.6	25667 \pm 110	29448 - 30270	29819	29.86 \pm 0.41
SL15BM04_R	D-AMS 16785	42.84256	120.59393	1402.1 \pm 2.0	-10.1	17663 \pm 53	21102 - 21608	21370	21.36 \pm 0.25
Excluded due to location/elevation									
SLT3-1B	D-AMS 013010	43.00600	120.77000	1316.8 \pm 0.1	1.0	12533 \pm 42	14473 - 15106	14838	14.79 \pm 0.32
SL15JH07	D-AMS 013015	42.84211	120.59363	1407.0 \pm 2.0	-2.6	12072 \pm 47	13770 - 14072	13916	13.92 \pm 0.15
SL15JH07_R	D-AMS 16781	42.84211	120.59363	1407.0 \pm 2.0	0.0	11712 \pm 41	13438 - 13605	13522	13.52 \pm 0.08
Excluded due to duplicate excluded									
SL15AE05_R	D-AMS 16786	43.05017	120.65868	1343.7 \pm 2.0	6.0	12273 \pm 373	14034 - 14403	14179	14.22 \pm 0.18
SLT1-2C-1_R	D-AMS 16787	43.02515	120.70330	1344.5 \pm 2.0	8.0	12288 \pm 37	14054 - 14460	14202	14.26 \pm 0.20
Samples not in bold were further excluded from my study									

Standard procedures for shells include examining for evidence of secondary calcite deposits such as caliche that may contaminate the sample. If a thin, friable layer of secondary calcite was observed, it would be scraped away with a blade. The thickest part of the shell was selected for dating, then heated in sufficient 0.1 M HCl to etch away approximately 30% of total mass. For tufa samples, the thickest representative interior portion of the largest fragment, or several representative small pieces, were weighed and then heated in sufficient 0.1 M HCl to etch away approximately 30% of the total mass. This wash is a necessary step in order to remove possible contamination. Direct AMS utilized the AMS method to determine radiocarbon ages for this study and followed procedures described by Zoppi (2010).

Assuming a carbonate sample has carbon originally fixed from the atmosphere, the rate in which ^{14}C ($t_{1/2} = 5.73$ ky) decays into ^{14}N is used to calculate a radiocarbon age. The production and reservoir of ^{14}C has not been constant through time, requiring radiocarbon ages to be recalibrated using calibration data sets to be corrected, as the dates could differ thousands of years than the true age. Two complications can occur with carbonate samples when radiocarbon age dating. A carbonate sample may have incorporated an abundant quantity of “dead” carbon, causing the dates to be much older than they really are. Another complication may be that the tufa carbonate sample was not dense, allowing the framework to be susceptible to modern atmospheric carbon effects. The hydrochloric acid wash at the beginning of the age dating process is meant to remove the possibility of these complication contaminations.

Radiocarbon ages were calibrated using CALIB Radiocarbon Calibration version 7.1, based upon robust radiocarbon calibration curves (Stuvier et al., 2017).

LiDAR-Based Mapping

I mapped paleoshorelines and fault scarps using 1-m LiDAR elevation data acquired by the University of Alaska-Fairbanks (UAF) and Department of Oregon Geology and Mineral Industries (DOGAMI), and 10-m digital elevation models (DEM) from the National Elevation Dataset (NED). From these DEMs, I derived shaded-relief and slope maps. Shaded-relief images were produced using various sun angles and azimuths to best illuminate features of interest.

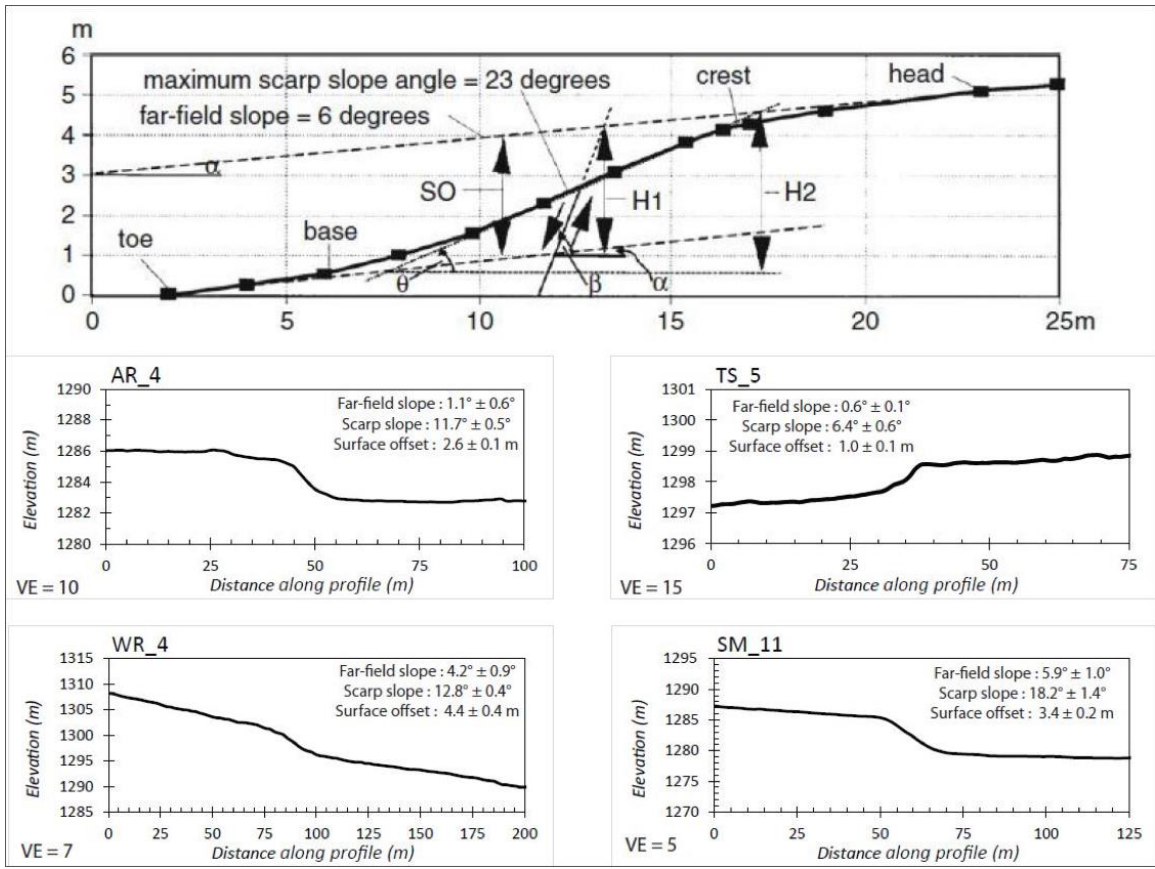
On a basemap of shaded-relief and slope maps, paleoshorelines were mapped by hand as precisely as possible at the riser crest, where the bench surface meets the erosional scarp (**Error! Reference source not found.**). Prominent shorelines were defined as a protuberant landform that is continuous, well-developed, and can be traced for at least 1 km (Figure 4). Fault scarps were mapped at the scarp crest (Figure 6) with the aid of slope shaded-relief.

Calculating Offset

The mapped fault scarps and paleoshorelines are utilized in this study as two different methods of addressing surface offsets and slip rates.

Surface offset for fault scarps were determined by topographic profiles that were drawn perpendicular to the mapped fault scarps. A total of 62 topographic profiles were extracted (Plate I) along the basin. Using standard equations (Figure 6), I calculated surface offset using the method of Amos et al. (2010) for the Winter Ridge, Slide Mountain, Ana River, and Thousand Springs faults (Appendix A).

Surface offset for paleoshorelines were calculated by determining the elevational differences between the highest highstand in several locations around the basin.



Error! Reference source not found.

Paleoshoreline elevations that differed by more than 2 m along the several locations were an indication of deformation (Hopkins and Dawers, 2016), most likely due to offset along a fault in Summer Lake. LiDAR-derived digital elevation models (DEM) were utilized to determine the elevational differences.

Calculating Slip Rates

By utilizing the surface offset measured by paleoshorelines, geochronology ages dated from paleoshorelines, and fault dip measurements of 60°, 70°, and 80°, slip rates were calculated for the Summer Lake basin. Although structural data on the WRF system has not been published, Pezzopane (1993) inferred a steep fault dip for the Ana River fault. Uncertainties were determined using standard equations (Taylor, 1997).

CHAPTER 4

RESULTS

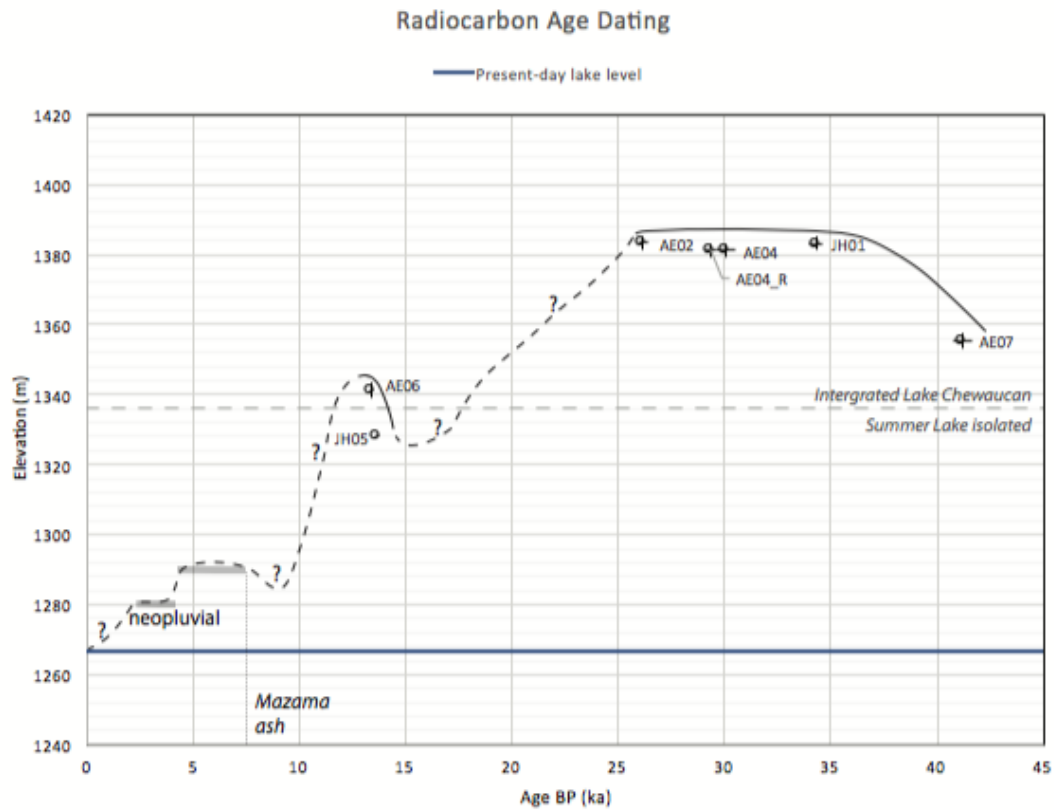
Radiocarbon Dating

Measured and calibrated radiocarbon ages for all 24 shoreline tufa samples (18 samples plus six duplicates) are shown in **Error! Reference source not found.**, with locations in Plate I. Calibrated radiocarbon ages range from 12.85 ± 0.12 ka BP to 41.19 ± 0.48 ka BP (2σ uncertainty). One sample had a radiocarbon age greater than the maximum theoretical age obtainable by radiocarbon dating (**Error! Reference source not found.**) and was excluded from further analysis. A duplicate of this sample was dated to 46.59 ± 0.78 ka BP, also near the upper limit of reliability for radiocarbon; the difference in these ages and the old age suggests that these are not reliable ages.

Error! Reference source not found.

Table 6. Percent differences between age ranges of duplicate samples				
Sample Name	Elevation (m)	Calibrated age (ka cal. BP) $\pm 2\sigma$ IntCal13	Age difference = $(A_1 - 2\sigma) - (A_2 + 2\sigma)$ (ka)	Percent difference = $\frac{((A_1 - 2\sigma) - (A_2 + 2\sigma))}{((A_1 - 2\sigma) * (A_2 + 2\sigma) / 2)}$
SL15BM04	1402.13 ± 2.0	29.86 ± 0.41		
SL15BM04_R	1402.13 ± 2.0	21.36 ± 0.25	7.84	31%
SL15JH06	1324.91 ± 0.1	26.36 ± 0.26		
SL15JH06_R	1324.91 ± 0.1	29.84 ± 0.37	2.85	10.2%
SL15JH07	1407.04 ± 2.0	13.92 ± 0.15		
SL15JH07_R	1407.04 ± 2.0	13.52 ± 0.08	0.17	1.2%
SL15AE04	1381.19 ± 2.0	30.09 ± 0.45		
SL15AE04_R	1381.19 ± 2.0	29.34 ± 0.28	0.02	0.1%
SL15AE05	1343.68 ± 2.0	14.67 ± 0.37		Agree within uncertainty
SL15AE05_R	1343.68 ± 2.0	14.22 ± 0.18	-0.1	
SLT1-2C-1	1322.4 ± 2.0	14.64 ± 0.36		Agree within uncertainty
SLT1-2C-1_R	1322.4 ± 2.0	14.26 ± 0.20	-0.18	

Samples not bolded are further excluded from my study



Error! Reference source not found.

Two discordant duplicate samples gave results that differed by >10% and were thus excluded from further analysis (Table 6). The remainder, although not within the calibrated uncertainty of each other, are within geologic uncertainty of the tufa formation process, as the growth of tufa can range from 0.1 mm/yr to ≥ 30 mm/yr (Rosen et al., 2004; Seard et al., 2013).

SLT3-1B sample location was within a rock quarry, rendering the initial in situ location difficult to determine, which resulted with the sample being excluded from further analysis.

Dated samples were also evaluated on the basis of their $\delta^{13}\text{C}$ (**Error! Reference source not found.**). The $^{13}\text{C}:^{12}\text{C}$ isotopic signature may indicate paleoenvironmental conditions of the water that the tufa precipitated from. Due to the long residence time of dissolved inorganic carbon (DIC) in closed-basin lakes, ^{12}C outgasses faster, leaving greater amounts of $\delta^{13}\text{C}$ in the water. Cohen (2000) obtained $\delta^{13}\text{C}$ results from stratigraphy of ostracod valves near the Ana River Canyon and Wetland Levees (**Error! Reference source not found.**). These samples ranged in $\delta^{13}\text{C}$ levels of -4.75 to 3.5 and -1 to 3.5 for the Ana River Canyon and Wetland Levees, respectively (Cohen et al., 2000), and are indicative of a closed-basin evaporitic lake. Therefore, samples outside of this range of $\delta^{13}\text{C}$ were further excluded from the study, as they may have been influenced by outside sources and do not represent the precipitative and evaporative fluctuations of the basin outlined in previous studies (**Error! Reference source not found.**) (Cohen et al., 2000).

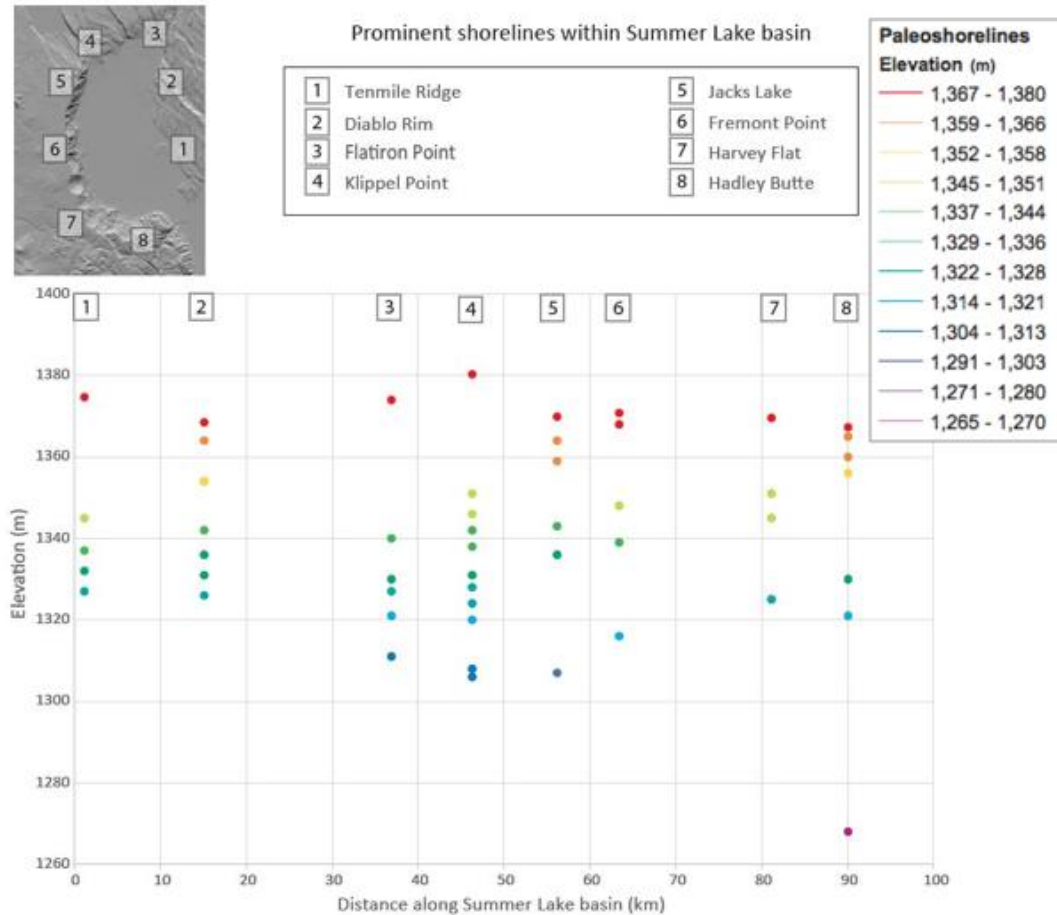
In **Error! Reference source not found.**, the age of seven remaining acceptable samples are plotted by elevation, representing a rough lake-level hydrograph. All seven of the samples lie east of the Thousand Springs fault in six sample locations (**Error! Reference source not found.** and Plate I). The age range for pluvial Lake Chewaucan's most recent highstand at ~1,340 m is 13.4 ± 0.1 to 13.7 ± 0.5 ka BP, with an average age of 13.5 ka BP (**Error! Reference source not found.**). In addition, our samples date an earlier and higher highstand approximately 26-34 ka at ~1,380 m.

Paleoshoreline Mapping

Mapping paleoshorelines can allow an age applied in one location to also be applied to another location further along the shoreline length. Locations of shoreline

sections are shown in **Error! Reference source not found.** while the detailed mapping of paleoshoreline features are shown in Plate I. Both the elevation range and the prominent shorelines are indicated in each area, and prominent shorelines are assumed to be correlated since they likely represent longer stillstands.

Mappable shorelines within the Hadley Butte section ranged from the highest elevation of 1,367.3 m to the base of Summer Lake basin at 1,266 m (Plate I). There are seven prominent shorelines ranging elevations from 1,365-1,321 m. The most prominent occur at 1,330 m, 1,356 m, and 1,360 m (**Error! Reference source not found.**).



Error! Reference source not found.

Mappable shorelines within the Harvey Flat section ranged from the highest elevation of 1,363.6 m to the base of Summer Lake basin (Plate I). There are at least six prominent shorelines ranging elevations from 1,369-1,325 m. The most prominent occur at 1,345 m and 1,351 m (**Error! Reference source not found.**).

Mappable shorelines within the Fremont Point section ranged from the highest elevation of 1,363.8 m to the base of Summer Lake basin (Plate I). There are seven prominent shorelines ranging elevations from 1,368-1,316 m. The most prominent occur at 1,316 m, 1,339 m, and 1,348 m (**Error! Reference source not found.**).

Mappable shorelines within the Jacks Lake section ranged from the highest elevation of 1,368.0 m to the base of Summer Lake basin (Plate I). There are ten prominent shorelines ranging elevations from 1,364-1,307 m. The most prominent occur at 1,336 m, 1,343 m, and 1,359 m (**Error! Reference source not found.**).

Mappable shorelines within the Klippel Point section ranged from the highest elevation of 1,380.3 m to the base of Summer Lake basin (Plate I). There are fifteen prominent shorelines ranging elevations from 1,380-1,306 m. The most prominent occur in two sets, one set is 1,338 m, 1,342 m, 1,346 m, 1,351 m, and a second set is 1,308 m, 1,320 m, 1,324 m, 1,328 m, and 1,331 m (**Error! Reference source not found.**).

Mappable shorelines within Flatiron Point section ranged from the highest elevation of 1,374.0 m to the base of Summer Lake basin (Plate I). There are seven prominent shorelines ranging elevations from 1,340-1,311 m. The most prominent occur at elevations 1,321 m, 1,327 m, and 1,330 m (**Error! Reference source not found.**).

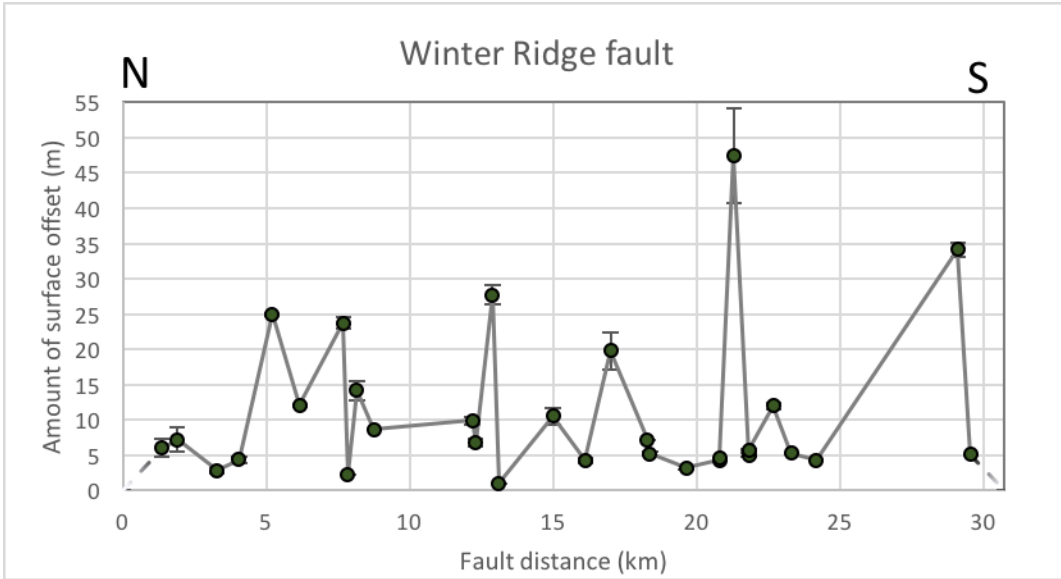
Mappable shorelines within the Diablo Rim section ranged from the highest elevation of 1,364.5 m to the base of Summer Lake basin (Plate I). There are seven prominent shorelines ranging elevations from 1,364-1,326 m. The most prominent occur at 1,331 m, 1,336 m, 1,342 m, and 1,354 m (**Error! Reference source not found.**).

Mappable shorelines within the Ten-Mile Ridge section ranged from the highest elevation of 1,374.1 m to the base of Summer Lake basin (Plate I). There are eleven prominent shorelines ranging elevations from 1,374-1,327 m. The most prominent occur at 1,332 m, 1,337, and 1,345 m (**Error! Reference source not found.**).

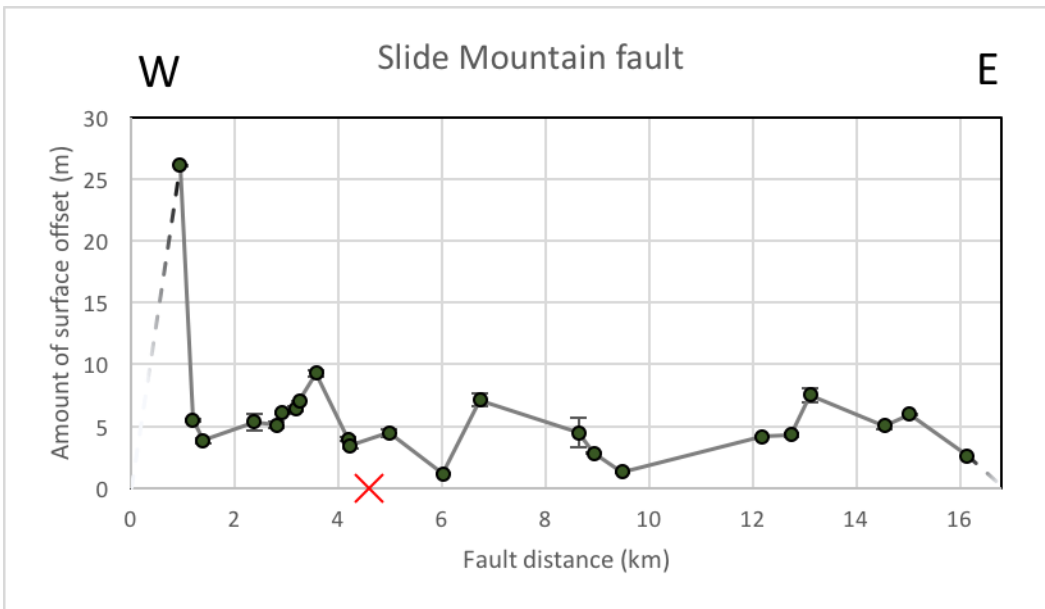
Outside of these mapped sections, shorelines either did not form, were not well-preserved because of erosion and/or human activity, or destroyed by landslide debris. Wind patterns largely contribute to the formation, or lack of formation, of paleoshorelines and shoreline tufa precipitates. The Summer Lake basin lies within the belt of westerlies; it appears that this was the case during the Pleistocene as well. This wind pattern results in greater wave action on the eastern margin of the lake, creating conditions that promote both paleoshoreline formation and growth of shoreline tufa, as well as the relative lack of tufa on the western margin of the basin. In addition, on the western margin, landslides that occurred while the lake was in place would have destroyed shorelines and perhaps limited the amount of time available for new features to form.

Fault Scarp Topographic Profiles and Surface Offset

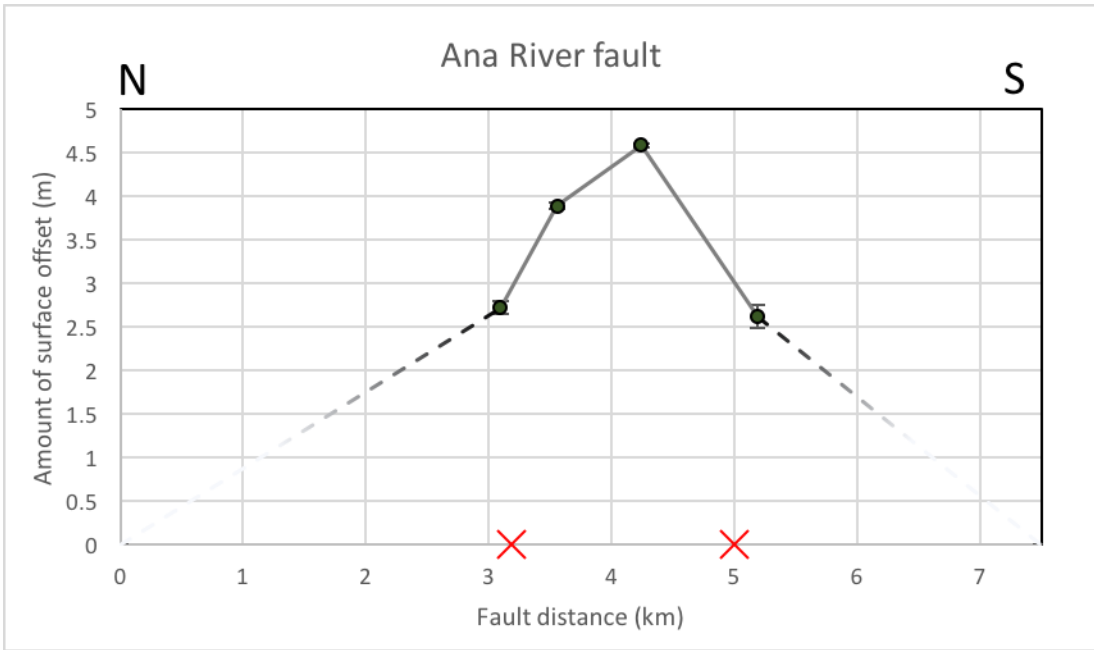
Although the western margin of the basin does not host many prominent shorelines, there are many prominent fault scarps. While shoreline offset allows us to measure basin-wide deformation, fault scarps focus in on a single feature within the basin. Of the topographic profiles measured within the Summer Lake basin, fault scarps



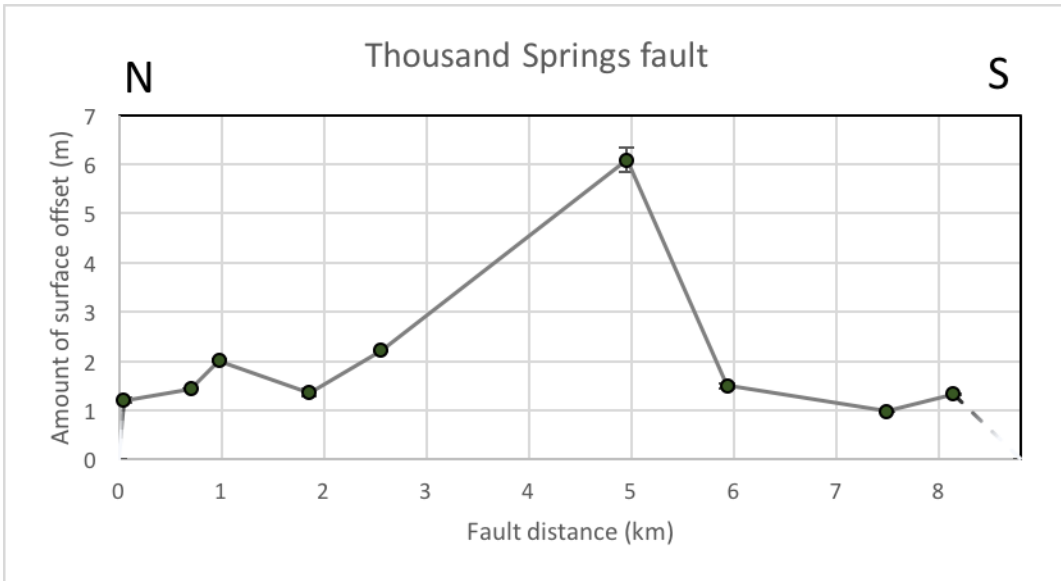
Error! Reference source not found.



Error! Reference source not found. fault segment. Paleoseismic trench location (Pezzopane, 1993) indicated by red X.



Error! Reference source not found.



Error! Reference source not found.

generally appear simple, some with grabens or hanging-wall rollback. In Figure 6 there are four topographic profiles depicting the average simple fault scarp topographic profile typical from each segment of the WRF system and the Thousand Springs fault.

Fault scarp surface offset is plotted along the length of the Winter Ridge, Slide Mountain, Ana River, and Thousand Springs faults and shown in **Error! Reference source not found.**, **Error! Reference source not found.**, **Error! Reference source not found.**, and **Error! Reference source not found.**. The locations of topographic profiles are shown in Plate I; measurements and calculations used to derive these plots are located in Appendix A.

Error! Reference source not found. depicts the surface offset across 30 fault scarp topographic profiles along the 29.5-km long Winter Ridge fault segment (Plate I). The greatest surface offset measurement (47.4 ± 6.7 m) was excluded from further analysis from the Winter Ridge fault segment because it is a bedrock scarp, and thus not representative of the most recent earthquakes. Total surface offset ranges from 1.0 ± 0.1 m to 34.1 ± 1.0 , with an average surface offset of 9.7 m. The second largest surface offset of 34.1 ± 1.0 m is located 1.6 km from the Slide Mountain fault segment boundary (Plate I). With the exception of two topographic surface offset measurements, 6.0 ± 1.3 m and 7.2 ± 1.7 m, the uncertainties represent less than 15% error of the values.

Error! Reference source not found. depicts the surface offset for 23 fault scarp topographic profiles along the 16.1-km long Slide Mountain fault segment (Plate I). Total surface offset ranges from 1.1 ± 0.1 to 26.1 ± 0.1 m, with an average surface offset of 5.8 m. The largest surface offset, 26.1 ± 0.1 m, is located 1.0 km from the Winter Ridge fault

segment (Plate I). With the exception surface offset values 4.5 ± 1.2 m and 5.3 ± 0.7 m, the uncertainties range up to 8% of the surface offset values.

Error! Reference source not found. depicts the surface offset for four fault scarp topographic profiles along the 7.5-km long Ana River fault segment (Plate I). Total surface offset ranges from 2.6 ± 0.1 m to 4.6 ± 0.1 m with an average surface offset of 3.4 m. The uncertainties are all within 5% of their surface offset values.

Error! Reference source not found. depicts the surface offset for five fault scarp topographic profiles along the length of the 8.1-km long Thousand Springs fault (Plate I). The total surface offset values range between 1.2 ± 0.7 m to 2.2 ± 0.1 m, with an average surface offset of 1.6 m. The uncertainties for these values represent error within 7% of their surface offset values.

With the seven radiocarbon-dated paleoshoreline tufas, the surface offset of paleoshorelines determined by elevational differences, and the surface offset from the faults scarps, I will be able to address the spatial and temporal variation in surface offsets and slip rates in the Summer Lake basin.

CHAPTER 5

DISCUSSION

Comparing Fault Scarp-Based Slip Distribution Data with Historical Events

Slide Mountain Fault Segment

The average fault scarp-based surface offset for the Slide Mountain fault segment is 5.8 m (**Error! Reference source not found.**), representing more than one surface-rupturing event. **Error! Reference source not found.** shows the average vertical offset recorded during one historical event. The Slide Mountain fault segment is approximately 16.1 km long (**Error! Reference source not found.**). Average displacement measured along the 14 km long Warm Springs segment during the Borah Peak earthquake is 1.4 m (**Error! Reference source not found.**). Assuming a similar average displacement for a single event, I can calculate the likely number of events on the Slide Mountain fault segment by dividing 5.8 m by 1.4 m, which is approximately four. Therefore, it is reasonable to estimate that there have been approximately three to five surface-rupturing events, most likely since earlier higher highstand that occurred approximately 26.2 ± 0.2 to 34.3 ± 0.3 ka BP (**Error! Reference source not found.**).

The Dixie Valley/Fairview earthquake ruptured in segments, and two of the segments, Westgate and Gold King, are comparable in rupture length with the fault length of Slide Mountain (16.1 km) (**Error! Reference source not found.**). Westgate (18 km) and Gold King (16 km) fault segments had average displacements of approximately 0.4 m and 0.45 m, respectively (**Error! Reference source not found.**). Comparing the average surface offset with Slide Mountain average displacement (5.8 m), those offsets

would suggest that there have been approximately 12 and 15 surface-rupturing events since ~26-34 ka BP. Crone et al. (2009) estimates that the WRF system has a recurrence interval (RI) of 3.1 ky, based on the trench data from the ARF and SMF. This data suggests a recurrence interval of 1.7-3.0 ky for the Slide Mountain fault segment, and based on the faults orientation to current stress field, I find this range too fast.

Winter Ridge Fault Segment

The average fault scarp-based surface offset for the 29.5 km long Winter Ridge fault segment is 9.7 m, clearly representing multiple surface-rupturing events (**Error! Reference source not found.** and **Error! Reference source not found.**). But how many? Average displacement measured along the 36 km long Lost River Range during the Borah Peak earthquake is 1.82 m (**Error! Reference source not found.**). Assuming a similar average displacement for a single event, I can calculate the likely number of events on the Winter Ridge fault segment by dividing 9.7 by 1.8, which is approximately five. As these surface-rupturing events occurred after the highest highstand, with ages ranged between 26.2 ± 0.2 to 34.3 ± 0.3 ka BP, it is reasonable to estimate that there have been four to six surface-rupturing events since the last highest highstand. Crone et al. (2009) estimated WRF system's RI of 3.1 ky, however, Langridge (1998) determined that the most recent eight surface-rupturing events recorded at ARF had a recurrence interval of ~11 ky. Therefore, since ~26–34 ka BP, it is reasonable that there have been four to six surface-rupturing events with a RI of 4.3–8.6 ky.

Badgers and Watters (2004) estimated that the Winter Ridge-Slide Mountain fault was capable of producing a ~M 7 earthquake. The Dixie Valley earthquake was M_s 6.8 and the average displacement was 0.9 m. Assuming a similar average displacement for a

single event, I can calculate the likely number of events on the Winter Ridge fault segment by dividing 9.7 m by 0.9 m, which is approximately 11. Therefore, it is not reasonable to estimate that there have been 10 to 12 surface-rupturing events since the last highest highstand ~26–34 ka BP. The recurrence interval for Winter Ridge fault segment, 2.2–3.4 ky, compares reasonably with Crone et al. (2009) RI estimation of 3.1 ky. However, the RI calculated for the Winter Rim Fault system (Crone et al., 2009) was based on limited data. The total fault length for Dixie Valley was 43-47 km, while the Winter Ridge and Slide Mountain are a continuously connected arcuate fault segment with a total fault length of 45.6 km.

The Winter Ridge fault segment of the WRF system and the Pearce fault segment of the Pleasant Valley fault system both have the greatest amount of fault length, 29.5 km and 30 km, and average vertical displacement, 9.7 m and 2.8 m, when compared to their respective fault segments, respectively (**Error! Reference source not found.**). Assuming a similar average displacement for the Winter Ridge fault for a single event as the Pearce fault, I can calculate the likely number of events on the Winter Ridge fault segment by dividing 9.7 m by 2.8 m, which is approximately four. Since ~26-34 ka BP, it is reasonable to estimate that there have been three to five surface-rupturing events.

The Winter Ridge fault segment is currently most favorably oriented to slip in the current stress field of the NWBR, while the Slide Mountain fault segment is oriented perpendicular to the current stress field (**Error! Reference source not found.** and **Error! Reference source not found.**). This may explain why the average slip on the Slide Mountain fault is approximately 50% less than average slip on the Winter Ridge fault (**Error! Reference source not found.** and **Error! Reference source not found.**).

Ana River Fault Segment

The average fault scarp-based surface offset for the Ana River fault segment is 3.4 m (**Error! Reference source not found.**). The Ana River segment is approximately 7.5 km long (**Error! Reference source not found.**). Pezzopane and Weldon (1993) also measured topographic profiles and the average surface displacement was 3.25 m. Event I and II are very well constrained for the Ana River fault, as the youngest events occurred post-lake between 2.12-4 to 7.6 ka BP and 12 to 14 ka BP (Langridge, 1998). Langridge (1998) estimated that the most recent event that cause surface-rupturing on the Ana River fault segment is had an average displacement of 1.25 m. Assuming a similar average displacement for a single event, I can calculate the likely number of events on the Ana River fault segment by dividing 3.4 m by 1.25 m, which is approximately three. Therefore, this displacement may represent between two and three events since 13.4–13.7 ka BP. Langridge (1998) described the surface-rupturing events of the Ana River fault segment, and that the Event III was bracketed between 12 and 15 ka BP. Therefore, it is reasonable for two or three events since the most recent highstand in 13.4–13.7 ka BP.

Thousand Springs Fault

The average fault scarp-based surface offset for the Thousand Springs fault is 1.6 m (**Error! Reference source not found.**). The Thousand Springs fault is approximately 8.1 km long (**Error! Reference source not found.**). Average displacement measured along the 8.5 km long Tobin fault segment during the Pleasant Valley earthquake is 1.9 m (**Error! Reference source not found.**). Making the assumption that the surface-rupturing events of the Thousand Springs fault occurred post-lake, due to their geomorphic appearance, I assume that sediments are approximately 2.12-4 ka BP. Langridge (1998)

determined that Event III for the Ana River fault was the last sub-Lacustrine earthquake, which brackets the maximum age to 12-15 ka BP. Therefore, I suggest it is reasonable that there have been one or two events on the Thousand Springs fault between 2.12-4 and 12-15 ka BP.

Within the slip distributions for each fault and fault segment, there is a range of variability in value of the surface offset by function of fault length. For example, the following are eight surface offset measurements along 7.8 km of the Winter Rim fault segment: 6.0 m, 7.2 m, 2.9 m, 4.4 m, 25.0 m, 12.1 m, 23.7 m, and 2.3 m (Appendix A, WR1-WR8). The variability between one measurement and the next, and the possibility of measurements missing entirely may be due how well the fault scarp is preserved because of erosion and/or human activity, or destroyed by landslide debris. Inherently due to high-resolution LiDAR, measurements of surface offset do not have much uncertainty within their measurements.

Comparing Fault Scarp-Based Slip Distribution with Local Events

Egger et al. (in review) reported the surface offset measured from 78 Surprise Valley topographic profiles fault scarps ranged between 0.8 and 22.2 m. With further analysis, the average total surface offset for all topographic profiles was approximately 4.1 m and approximately 2.4 m for the estimated most recent event surface offset event (Egger et al., in review).

Personius et al. (2009) discovered through means of trenching and stream exposures that there had been at least five surface-rupturing events with estimated rupture lengths of 53-65 km and displacement estimates of 24.5 ± 1 m. This is indicative that the most surface offset from a rupturing event is <5 m within this particular tectonic setting.

Five surface-rupturing events would have approximately 1 m of displacement per event. Assuming a similar average displacement for a single event of 2.4 m, I can calculate the likely number of events on Surprise Valley fault by dividing 22.2 by 2.4, which is approximately nine events. The most recent event 1.2 ± 0.1 ka BP recorded offsets ranging between 0.6 to 4.9 m in the alluvial fan deposits (Egger et al., in review).

Comparing Paleoshoreline-Based Surface Offsets with Local Events

Surprise Valley also hosted a pluvial lake in the Pleistocene (**Error! Reference source not found.**); these fault systems both lie within the NWBR and thus are in similar tectonic settings. Marion (2016) calculated average offset of paleoshorelines of the Surprise Valley fault (SVF) using LiDAR-based mapping. Measured paleoshoreline offset was greatest in the central section of the SVF and gradually diminished near the fault tips (Marion, 2016). Marion (2016) also states that slip was distributed asymmetrically, with the largest amount of offset in the central section closer to the southern extent of the fault than the northern portion. The total offset measured by paleoshorelines was greater for SVF when compared to total offset measured by fault scarps. Marion (2016) reasons this may be due to the nature of how geomorphic features degrade or it could be attributed to a larger structural discontinuity between the northern and central portions.

The average displacement measured for the shorelines of Surprise Valley, mapped in three sections, were 5.3 m in the north, 14.4 m in the center, and 4.7 m in the south (Marion, 2016). The WRF system slip and total offset is also distributed asymmetrically. The northern segment, Ana River, had an average of 3.4 m of displacement. The central segment, also the longest segment, Winter Ridge, had the highest average of

displacement at 9.7 m. The southern section, Slide Mountain, and 5.8 m of average displacement, and the Thousand Springs fault had 1.6 m. There could be changes in the substructure that may attribute to WRF system asymmetrical offset.

Comparing Deformation with Catlow Valley

The Catlow Valley (Figure 2) is a nearby analog where shorelines were studied and found to be deformed (Hopkins and Dawers, 2016). There are no fault scarps within the area. However, the elevation of the shorelines changes more abruptly near breached ramps, which the authors interpret as deformation along faults that do not reach the surface. Also within this study, Hopkins and Dawers (2016) established a window of inherent variability in elevations of shorelines as it developed and how deviation from this window may suggest tectonic deformation.

Paleoshoreline-Based Slip Rate Calculations

Slip rates are calculated by dividing the paleoshoreline-based surface offsets by the age date of when the offset occurred. As a pluvial lake formed paleoshorelines, they

Error! Reference source not found.

source not found., Error! Reference source not found., and Error! Reference source not found.). A 60° fault dip represents the standard mechanics of a normal fault in an extensional environment. A 70° fault dip was used by a geologic modeling company for the Ana River fault, and an 80° fault dip represents a steep fault in this study. The resulting slip rates for this study range from 0.18 mm/yr to 0.74 mm/yr (Table 8, Table 9, Table 10, Table 11, Table 12, Table 13, and Table 14).

Since all paleoshoreline offsets were being compared to the highest highstand—located at Klippel Point, the paleoshoreline offsets calculated for Flatiron Point, Diablo Rim, and Ten Mile Ridge cross multiple faults. Between Klippel Point shorelines and the other three locations, the Ana River fault and Thousand Springs fault dip towards each other, creating a graben in between them. Correlating shorelines across the basin, with two opposing angled faults, means that I'm not calculating slip rates for

Error! Reference source not found.

Table 8. Ten-mile Ridge paleoshoreline highstand offset rate over		TSF and ARF		
Klippel Pt (1380.3 m) - Ten-mile Ridge	6.2	Slip rates at fault dip angle		
		60 °	70°	80°
Lower age range (ka BP)	13.39	0.53	0.49	0.47
Upper age range (ka BP)	13.67	0.52	0.48	0.46
Average age (ka BP)	13.53	0.53	0.49	0.47

Error! Reference source not found.

Table 9. Diablo Rim paleoshoreline highstand offset rate over		TSF and ARF		
Klippel Pt (1380.3 m) - Diablo Rim (1364.5 m)=	15.8	Slip rates at fault dip angle (mm/yr)		
		60°	70°	80°
Lower age range (ka BP)	13.39	1.36	1.26	1.20
Upper age range (ka BP)	13.67	1.33	1.23	1.17
Average age (ka BP)	13.53	1.35	1.24	1.19

Error! Reference source not found.

Table 10. Flatiron Point paleoshoreline highstand offset rate over		TSF and ARF		
Klippel Pt (1380.3 m) - Flatiron Point (1374.0	6.3	Slip rates at fault dip angle (mm/yr)		
		60°	70°	80°
Lower age range (ka BP)	13.39	0.54	0.50	0.48
Upper age range (ka BP)	13.67	0.53	0.49	0.47
Average age (ka BP)	13.53	0.54	0.50	0.47

Error! Reference source not found.

Table 11. Jacks Lake paleoshoreline highstand offset rate over		WRF segment		
Klippel Pt (1380.3 m) - Jacks Lake (1368.0 m)=	12.3	Slip rates at fault dip angle (mm/yr)		
		60°	70°	80°
Lower age range (ka BP)	13.39	1.06	0.98	0.93
Upper age range (ka BP)	13.67	1.04	0.96	0.91
Average age (ka BP)	13.53	1.05	0.97	0.92

Error! Reference source not found.

Table 12. Fremont Point paleoshoreline highstand offset rate over		WRF segment		
Klippel Pt (1380.3 m) - Fremont Point (1363.8	16.5	Slip rates at fault dip angle (mm/yr)		
		60°	70°	80°
Lower age range (ka BP)	13.39	1.42	1.31	1.25
Upper age range (ka BP)	13.67	1.39	1.28	1.23
Average age (ka BP)	13.53	1.41	1.30	1.24

Error! Reference source not found.

Table 13. Harvey Flat paleoshoreline highstand offset rate over		WRF segment		
Klippel Point (1380.3 m) - Harvey Flat (1363.6 m)=	16.7	Slip rates at fault dip angle (mm/yr)		
		60°	70°	80°
Lower age range (ka BP)	13.39	1.44	1.33	1.27
Upper age range (ka BP)	13.67	1.41	1.30	1.24
Average age (ka BP)	13.53	1.43	1.31	1.25

Error! Reference source not found.

Table 14. Hadley Butte paleoshoreline highstand offset rate over		WRF segment		
Klippel Point (1380.3 m) - Hadley Butte (1367.3 m)=	13.0	Slip rates at fault dip angle (mm/yr)		
		60°	70°	80°
Lower age range (ka BP)	13.39	1.12	1.03	0.99
Upper age range (ka BP)	13.67	1.10	1.01	0.97
Average age (ka BP)	13.53	1.11	1.02	0.98

any shoreline locations east of the Winter Ridge fault. Instead, I am calculating an offset rate. While I cannot differentiate which fault, the Ana River fault segment or the Thousand Springs fault, slipped more or less to each other, I do know that they are not slipping at the same rate. If they were, the net offset between shorelines in Jacks Lake and Diablo Rim would be zero. From the shoreline elevations, I know that the eastern block is relatively lower than the western block. However, the shoreline data appear to indicate that both the western and eastern block (and graben) are relatively higher to the north than to the south.

Offset rates ranged from 0.18-0.27 mm/yr, 0.47-0.70 mm/yr, and 0.19-0.28 mm/yr for Ten Mile Ridge, Diablo Rim, and Flatiron Point (**Error! Reference source not found., Error! Reference source not found., and Error! Reference source not found.**), respectively, but it is not possible to determine how the slip is accommodated between the two faults. While noting that the Ana River fault has been estimated a slip rate of 0.2-0.3 mm/yr (Langridge, 1998), the Thousand Springs fault dips in the opposite direction, and without additional age constraints, it is not possible to determine slip rates for the Ana River fault by itself with current data.

Slip rates determined for the Winter Ridge fault segment range between 0.36-0.54 mm/yr in Jacks Lakes, 0.49-0.73 mm/yr in Fremont Point, 0.49-0.74 in Harvey Flat, and 0.38-0.57 mm/yr in Hadley Butte (**Error! Reference source not found., Error! Reference source not found., Error! Reference source not found., and Error! Reference source not found.**). These slip rates are comparable to those calculated for Slide Mountain, 0.4-0.6 mm/yr (Pezzopane and Weldon, 1993), and Winter Ridge, 0.3-0.4 mm/yr (Travis, 1977). Slip rates of <1 mm/yr are reasonable for the Summer Lake basin. This may also be due to the high-resolution LiDAR that was used to obtain the data, as this study is the first to use LiDAR to determine offsets of shorelines and fault scarps.

It is important to note that there are assumptions to be made when the two correlating shoreline locations are not directly across one fault from each other. The most important assumption is that paleoshorelines on either side of the basin have been correctly correlated. When correlating shorelines, the two keys are understanding the sequences of the shorelines, the highest shoreline at each location is the highest shoreline,

and it may be at different elevations due to deformation. The other key is to be able to recognize the geomorphic identity of each shoreline within the sequence. Features such as how prominent or extensive to each other further my confidence in correctly correlating shorelines. While the high resolution of the LiDAR made subtle features more apparent than they would in the field, there may be more faults in the basin where slip could be occurring, and the resulting rate I've calculated would be a sum of rates across multiple faults.

A few of these slip rates are higher than those that have been previously published. There are a few possibilities that could have resulted from the use of my methods. First, the highstand shorelines may not have been correctly correlated, producing an apparent offset in shorelines that were in reality of two different ages. This would affect the shoreline offset calculation, either over compensating for offset, or not representing the maximum highstand. The age used maybe also be incorrect, which is currently the age of the last pluvial highstand from radiocarbon data from this study. I am not sure which of these factors are incorrect, but it is unreasonable for the Winter Rim Fault system to have a slip rate > 1 mm/yr.

Slip rates estimated for Surprise Valley by Personius (2009) is approximately 0.6 ± 0.1 mm/yr. Marion (2015) used the same methods as this study and calculated paleoshoreline slip rates that ranged from 0.25 ± 0.02 mm/yr in the north, 1.07 ± 0.05 mm/yr in the center, and 0.36 ± 0.04 mm/yr in the south (Marion, 2016). The overall range of slip rates between the Summer Lake basin and Surprise Valley are comparable.

CHAPTER 6

CONCLUSION

By combining offset of paleoshorelines with radiocarbon dating of tufa, surface and high-resolution Light Detection and Ranging (LiDAR)-derived elevation data, I was able to calculate paleoshoreline-based surface offsets and dip slip rates for the WRF system. With surface offsets from the fault scarp topographic profiles, I was able to determine slip distributions and compare those to historical surface-rupturing events. How do surface offset and slip rates vary spatially and temporally within the Summer Lake basin? Although there have not been historical seismicity records for northwestern Basin and Range faults, the spatial and temporal variance was addressed by comparing data derived from this study with historical and local events. By comparing historical records of slip distribution with surface offsets determined from fault scarp topographic profiles utilizing the method by Amos et al. (2010), reasonable comparisons were made.

The USGS estimated the Winter Rim fault system to have a slip rate of 0.43 mm/yr, based on trench data from Ana River and Slide Mountain fault segments (Crone et al., 2009). From this study, I presented slip rates that ranged between 0.18 to 0.74 mm/yr, which lie squarely in the middle of Crone et al (2009) published range. As these slip rates vary spatially and temporally, selecting a single slip rate or an average would not represent the seismic hazard of the entire fault system. While the Winter Rim fault system is limited in the sense of radiocarbon dating, due to the lack of paleoshoreline tufa growth around the basin, this study produced a new set of radiocarbon-dated tufa ages. This method has proven successful in nearby Surprise Valley, CA (Marion, 2016) and the

Alvord basin, OR (Oldow and Singleton, 2008), providing an opportunity for obtaining surface offsets and dip slip rates through means other than trenching.

REFERENCES

- Adams, K.D., Wesnousky, S.G., and Bills, B.G., 1999, Isostatic rebound, active faulting, and potential geomorphic effects in the Lake Lahontan basin, Nevada and California: *Bulletin of the Geological Society of America*, v. 111, p. 1739–1756, doi: 10.1130/0016-7606(1999)111<1739:IRAFAP>2.3.CO;2.
- Allison, I.S., 1982, *Geology of Pluvial Lake Chewaucan, Lake County, Oregon*: Corvallis, Oregon State University Press, 79 p.
- Badger, T.C., and Watters, R.J., 2004, Gigantic seismogenic landslides of Summer Lake basin, south-central Oregon: *Geological Society of America Bulletin*, v. 116, p. 687–697, doi: 10.1130/B25333.1.
- Barrientos, S.E., Stein, R.S., and Ward, S.N., 1987, Comparison of the 1959 Hebgen Lake, Montana and the 1983 Borah Peak, Idaho, earthquakes from geodetic observations: *Bulletin of the Seismological Society of America*, v. 77, p. 784–808.
- Caskey, S.J., Wesnousky, S.G., Zhang, P., and Slemmons, D.B., 1996, Surface Faulting of the 1954 Fairview Peak (M 7.7) and Dixie Valley (M 6.8) Earthquakes, Central Nevada: *Bulletin of the Seismological Society of America*, v. 86, p. 761–787.
- Cohen, A.S., Palacios-fest, M.R., Negrini, R.M., Wigand, P.E., and Erbes, D.B., 2000, A paleoclimate record for the past 250,000 years from Summer Lake, Oregon, USA: II. Sedimentology, paleontology and geochemistry: *Journal of Paleolimnology*, v. 24, p. 151–182.
- Crider, J.G., 2001, Oblique slip and the geometry of normal-fault linkage: mechanics and a case study from the Basin and Range in Oregon: *Journal of Structural Geology*, v.

23, p. 1997–2009.

Crittenden, M.D., 1963, New Data on the Isostatic Deformation of Lake Bonneville:

Geological Survey Professional Paper, v. 454–E, p. 31.

Crone, A., and Haller, K., 1991, Segmentation and the coseismic behavior of Basin and

Range normal faults: examples from east-central Idaho and southwestern Montana,

USA: *Journal of Structural Geology*, v. 13, p. 151–164, doi: 10.1016/0191-

8141(91)90063-O.

Crone, A.J., Haller, K.M., and Maharrey, J.Z., 2009, Evaluation of Hazardous Faults in

the Intermountain West Region—Summary and Recommendations of a Workshop:

USGS Open-File Report, v. 2009–1140, p. 72.

Crone, A.J., Machette, M.N., Bonilla, M.G., Lienkaemper, J.J., Pierce, K.L., Scott, W.E.,

and Bucknam, R.C., 1984, Surface faulting accompanying the Borah Peak

earthquake and segmentation of the Lost River fault, Central Idaho: *Geology*, v. 12,

p. 664–667, <http://www.bssaonline.org/content/77/3/739.abstract>.

DePolo, C.M., Clark, D.G., Slemmons, D.B., and Ramelli, A.R., 1991, Historical surface

faulting in the Basin and Range province, western North America: implications for

fault segmentation: *Journal of Structural Geology*, v. 13, p. 123–136, doi:

10.1016/0191-8141(91)90061-M.

Diggles, M.F., Conrad, J.E., and Soreghan, G.A., 1990, Geologic map of the Diablo

Mountain Wilderness Study Area, Oregon.:

Egger, A.E., Ibarra, D.E., Weldon, R., Langridge, R., Marion, B., and Hall, J. The

influence of pluvial lake cycles on earthquake recurrence in the northwestern Basin and Range, USA: GSA,.

Felton, A., Jewell, P.W., Chan, M., and Currey, D., 2006, Controls of Tufa Development in Pleistocene Lake Bonneville, Utah: *The Journal of Geology*, v. 114, p. 377–389, doi: 10.1086/501218.

Hampel, A., Hetzel, R., and Maniatis, G., 2010, Response of normal faults to glacial-interglacial fluctuations of ice and water masses on Earth's surface: *Philosophical Transactions of the Royal Society*, v. 368, p. 2501–2517, doi: 10.1098/rsta.2010.0031.

Hopkins, M.C., and Dawers, N.H., 2016, Vertical deformation of lacustrine shorelines along breached relay ramps, Catlow Valley fault, southeastern Oregon, USA: *Tectonophysics*, v. 674, p. 89–100, doi: 10.1016/j.tecto.2016.02.015.

Karow, T., and Hampel, A., 2010, Slip rate variations on faults in the Basin-and-Range Province caused by regression of Late Pleistocene Lake Bonneville and Lake Lahontan: *International Journal of Earth Sciences*, v. 99, p. 1941–1953, doi: 10.1007/s00531-009-0496-3.

Kreemer, C., Hammond, W.C., Geoffrey, B., Holland, A.A., and Bennett, R.A., 2012, A Geodetic Strain Rate Model for the Pacific-North American Plate Boundary, Western United States: Nevada Bureau of Mines and Geology, doi: 10.1130/B30150.1.Williams.

Langridge, R.M., 1998, Paleoseismic deformation in behind-arc lacustrine settings- Acambay, Mexico and Ana River, Oregon: University of Oregon, 188 p.

- Langridge, R.M., Pezzopane, S.K., and Weldon, R.J., 2001, Slip rate, recurrence intervals and paleoearthquakes for the Ana River Fault, central Oregon: Negrini, R., Pezzopane, S.K., and Badger, T. C., eds., Quaternary Studies near Summer Lake, Oregon, Friends of the Pleistocene, p. 126.
- Licciardi, J.M., 2001, Chronology of latest Pleistocene lake-level fluctuations in the pluvial Lake Chewaucan basin, Oregon, USA: *Journal of Quaternary Science*, v. 16, p. 545–553, doi: 10.1002/jqs.619.
- Marion, B.N., 2016, Spatiotemporal Slip Rate Variations Along Surprise Valley Fault in Relation to Pleistocene Pluvial Lakes:
- Negrini, R.M., Erbes, D.B., Faber, K., Herrera, A.M., Roberts, A.P., Cohen, A.S., Wigand, P.E., and Foit, F.F., 2000, A paleoclimate record for the past 250,000 years from Summer Lake, Oregon, USA: I. Chronology and magnetic proxies for lake level: *Journal of Paleolimnology*, v. 24, p. 125–149, doi: 10.1023/A:1008144025492.
- Nelson, S.T., Wood, M.J., Mayo, A.L., Tingey, D.G., and Eggett, D., 2005, Shoreline Tufa and Tufaglomerate from Pleistocene Lake Bonneville, Utah, USA: Stable isotopic and mineralogical records of lake conditions, processes, and climate: *Journal of Quaternary Science*, v. 20, p. 3–19, doi: 10.1002/jqs.889.
- Oldow, J.S., and Singleton, E.S., 2008, Application of Terrestrial Laser Scanning in determining the pattern of late Pleistocene and Holocene fault displacement from the offset of pluvial lake shorelines in the Alvord extensional basin, northern Great Basin, USA: *Geosphere*, v. 4, p. 536, doi: 10.1130/GES00101.1.

- Personius, S.F., Crone, A.J., Machette, M.N., Mahan, S. a., and Lidke, D.J., 2009, Moderate rates of late Quaternary slip along the northwestern margin of the Basin and Range Province, Surprise Valley fault, northeastern California: *Journal of Geophysical Research: Solid Earth*, v. 114, doi: 10.1029/2008JB006164.
- Pezzopane, S.K., 1993, *Active Faults and Earthquake Ground Motions in Oregon*: University of Oregon.
- Pezzopane, S.K., and Weldon, R.J., 1993, Tectonic Role of Active Faulting in Central Oregon: *Tectonics*, v. 12, p. 1140–1169.
- Reheis, M.C., Adams, K.D., Oviatt, C.G., and Bacon, S.N., 2014, Pluvial lakes in the Great Basin of the western United States - a view from the outcrop: *Quaternary Science Reviews*, v. 97, p. 33–57.
- Rosen, M.R., Arehart, G.B., and Lico, M.S., 2004, Exceptionally fast growth rate of less than 100-yr-old tufa, Big Soda Lake, Nevada: Implications for using tufa as a paleoclimate proxy: *Geological Society of America*, v. 32, p. 409–412, doi: 10.1130/G20386.1.
- Scott, W., Pierce, K., and Hait, M.H., 1985, Quaternary Tectonic Setting of the 1983 Borah Peak Earthquake, Central Idaho: *Bulletin of the Seismological Society of America*, v. 75, p. 1053–1066.
- Seard, C., Camoin, G., Rouchy, J., and Virgone, A., 2013, Composition, structure and evolution of a lacustrine carbonate margin dominated by microbialites: Case study from the Green River formation (Eocene; Wyoming, USA): *Paleogeography, Paleoclimatology, Paleoecology*, v. 382, p. 128–144, doi:

10.1016/j.palaeo.2013.04.023.

Stuvier, M., Reimer, P.J., and Reimer, R.W., 2017, CALIB 7.1: WWW program, <http://calib.org> (accessed January 2016).

Taylor, J., 1997, An Introduction to Error Analysis: 45-91 p.

Travis, P.L., 1977, Geology of the area near the north end of Summer Lake: Eugene, University of Oregon.

Treerotchananon, A., 2009, Extension between Major Faults, Central Oregon Basin and Range: University of Oregon, 1-71 p.

U.S. Geological Survey Earthquake Hazards Program, 2017, Latest Earthquakes: U.S. Geological Survey, <http://earthquake.usgs.gov/earthquakes/map/>.

Walker, G.W., 1963, Reconnaissance geologic map of the eastern half of the Klamath Falls (AMS) quadrangle, Lake and Klamath Counties, Oregon: U.S. Geological Survey Mineral Investigations Field Studies Map MF-260, 1 sheet, scale 1:250,000:

Wallace, R.E., Bonilla, M.G., and Villalobos, H.A., 1984, Faulting related to the 1915 earthquakes in Pleasant Valley, Nevada: USGPO, v. 1274–AB.

APPENDIXES

Appendix A

Appendix A. Table of topographic profile surface offset calculations.

Plate I. Shaded-relief map of Winter Rim Fault system in the Summer Lake basin, scale 1:36,000.